AFRL-RX-TY-TR-2010-0066

CARBON NANOTUBE REINFORCED FLEXIBLE WINDOWS FOR BLAST PROTECTION

Mei Zhang, Richard Liang, Chuck Zhang and Ben Wang

Florida Agricultural and Mechanical University (FAMU)
Florida State University (FSU) College of Engineering
2525 Pottsdamer Street
Tallahassee, FL 32310

Contract No. FA4819-08-C-0009

JULY 2010

DISTRIBUTION A: Approved for public release; distribution unlimited.

AIR FORCE RESEARCH LABORATORY
MATERIALS AND MANUFACTURING DIRECTORATE

■ **Air Force Materiel Command** ■ **United States Air Force** ■ **Tyndall Air Force Base, FL 32403-5323**

DISCLAIMER

Reference herein to any specific commercial product, process, or service by trade name, trademark, manufacturer, or otherwise does not constitute or imply its endorsement, recommendation, or approval by the United States Air Force. The views and opinions of authors expressed herein do not necessarily state or reflect those of the United States Air Force.

This report was prepared as an account of work sponsored by the United States Air Force. Neither the United States Air Force, nor any of its employees, makes any warranty, expressed or implied, or assumes any legal liability or responsibility for the accuracy, completeness, or usefulness of any information, apparatus, product, or process disclosed, or represents that its use would not infringe privately owned rights.

NOTICE AND SIGNATURE PAGE

Using Government drawings, specifications, or other data included in this document for any purpose other than Government procurement does not in any way obligate the U.S. Government. The fact that the Government formulated or supplied the drawings, specifications, or other data does not license the holder or any other person or corporation; or convey any rights or permission to manufacture, use, or sell any patented invention that may relate to them.

This report was cleared for public release by the Air Force Research Laboratory Airbase Technologies Division Public Affairs Office and is available to the general public, including foreign nationals. Copies may be obtained from the Defense Technical Information Center (DTIC) (http://www.dtic.mil).

AFRL-RX-TY-TR-2010-0066 HAS BEEN REVIEWED AND IS APPROVED FOR PUBLICATION IN ACCORDANCE WITH ASSIGNED DISTRIBUTION STATEMENT.

10/21/2010

X SHEPPARD.PAUL.E.1229966037 Digitally signed by SHEPPARD.PAUL.E.1229966037 DN: c=US, o=U.S. Government, ou=DoD, ou=PKI, ou=USAF, cn=SHEPPARD.PAUL.E.1229966037 Date: 2010.10.22 09:53:05 -05'00'
Paul E Sheppard

PAUL E. SHEPPARD
Work Unit Manager

X MEEKER.SANDRA.RENEE.1230345607 Digitally signed by MEEKER.SANDRA.RENEE.1230345607 DN: c=US, o=U.S. Government, ou=DoD, ou=PKI, ou=USAF, cn=MEEKER.SANDRA.RENEE.1230345607 Date: 2010.10.21 14:14:18 -05'00'

SANDRA R. MEEKER
Chief, Airbase Engineering Development Branch

X

ALBERT N. RHODES, PH.D.
Chief, Airbase Tecchnologies Division

This report is published in the interest of scientific and technical information exchange, and its publication does not constitute the Government's approval or disapproval of its ideas or findings.

REPORT DOCUMENTATION PAGE

Form Approved
OMB No. 0704-0188

The public reporting burden for this collection of information is estimated to average 1 hour per response, including the time for reviewing instructions, searching existing data sources, gathering and maintaining the data needed, and completing and reviewing the collection of information. Send comments regarding this burden estimate or any other aspect of this collection of information, including suggestions for reducing the burden, to Department of Defense, Washington Headquarters Services, Directorate for Information Operations and Reports (0704-0188), 1215 Jefferson Davis Highway, Suite 1204, Arlington, VA 22202-4302. Respondents should be aware that notwithstanding any other provision of law, no person shall be subject to any penalty for failing to comply with a collection of information if it does not display a currently valid OMB control number.

PLEASE DO NOT RETURN YOUR FORM TO THE ABOVE ADDRESS.

1. REPORT DATE *(DD-MM-YYYY)*	2. REPORT TYPE	3. DATES COVERED *(From - To)*
31-JUL-2010	Final Technical Report	01-OCT-2008 -- 30-MAR-2010

4. TITLE AND SUBTITLE

Carbon Nanotube Reinforced Flexible Windows for Blast Protection

5a. CONTRACT NUMBER

FA4819-08-C-0009

5b. GRANT NUMBER

5c. PROGRAM ELEMENT NUMBER

99999F

6. AUTHOR(S)

Zhang, Mei; Liang, Richard; Zhang, Chuck; Wang, Ben

5d. PROJECT NUMBER

GOVT

5e. TASK NUMBER

F0

5f. WORK UNIT NUMBER

QF101009

7. PERFORMING ORGANIZATION NAME(S) AND ADDRESS(ES)

Florida Agricultural and Mechanical University - Florida State University
(FAMU-FSU) College of Engineering
2525 Pottsdamer Street
Tallahassee, FL 32310

8. PERFORMING ORGANIZATION REPORT NUMBER

9. SPONSORING/MONITORING AGENCY NAME(S) AND ADDRESS(ES)

Air Force Research Laboratory
Materials and Manufacturing Directorate
Airbase Technologies Division
139 Barnes Drive, Suite 2
Tyndall Air Force Base, FL 32403-5323

10. SPONSOR/MONITOR'S ACRONYM(S)

AFRL/RXQF, AFRL/RXQEM

11. SPONSOR/MONITOR'S REPORT NUMBER(S)

AFRL-RX-TY-TR-2010-0066

12. DISTRIBUTION/AVAILABILITY STATEMENT

Distribution Statement A: Approved for public release; distribution unlimited.

13. SUPPLEMENTARY NOTES

Ref AFRL/RXQ Public Affairs Case # 10-153. Document contains color images.

14. ABSTRACT

The objective of this program was to fabricate a carbon nanotube (CNT)-reinforced transparent plastic composite for use as a material for window or as a laminate layer in the blast-resistant glazed window. This program focused exclusively on assembling CNTs into highly organized structures and using CNT assemblies as a filler to reinforce the transparent plastic materials. This program demonstrated that using a highly organized CNT assembly such as CNT yarns as filler was an efficient way to improve the properties of polymeric composite while keeping the transparency of the composite. The reinforcement was significant. When using PMMA (poly(methyl methacrylate)) as the polymeric matrix, the modulus and strength of the composite increased linearly with the increase of CNT content. For the 17 wt% CNT-containing PMMA/CNT-yarn composite, compared to the neat PMMA sheet, the tensile strength, modulus, and toughness of the composite had a 5-fold, 10-fold, and 8-fold improvement, respectively. The composite had more than 40% transmittance even when the CNT content was 9 wt%. The technology developed in this program can be applied to other polymeric matrices.

15. SUBJECT TERMS

nanocomposite, carbon nanotube, yarn, nanofiller, modulus, strength, blast protection, window

16. SECURITY CLASSIFICATION OF:			17. LIMITATION OF ABSTRACT	18. NUMBER OF PAGES	19a. NAME OF RESPONSIBLE PERSON
a. REPORT	b. ABSTRACT	c. THIS PAGE			Paul Sheppard
U	U	U	UU	60	19b. TELEPHONE NUMBER *(Include area code)*

Reset

Standard Form 298 (Rev. 8/98)
Prescribed by ANSI Std. Z39.18

TABLE OF CONTENTS

LIST OF FIGURES

Figure **Page**

LIST OF TABLES

Table **Page**

ACKNOWLEDGEMENTS

This work was supported by the Air Force Research Laboratory, Airbase Technologies Division (AFRL/RXQ). We gratefully acknowledge the support and encouragement of Jennifer Robertson and Dave Scanland of AFRL/RXQ and Ian Welch, Applied Research Associates.

1. SUMMARY

Blast-resistant materials are desired for buildings and vehicles to protect facilities and people. Improving the blast resistance of the window is more challenging than that of the other parts of the building or vehicle since the requirement for transparency to visible light limits the materials and structures that can be applied. Transparent plastics are used as materials for window or as a laminate layer in the blast-resistant glazed window. It is obvious that further increasing the mechanical properties of transparent plastics would improve their ability for blast protection. The concept was to synthesize a special type of carbon nanotubes (CNTs), to assemble CNTs into highly organized structures, and to use CNT assemblies as filler to reinforce the transparent plastic materials.

The primary objectives of this work were to 1) optimize the method/process for synthesizing drawable CNT forests; 2) understand and improve the transformation of CNT forests into sheets and yarns; and 3) develop the processes to fabricate and characterize prototype CNT-reinforced polymer composites for blast-resistant applications.

The program investigated parameters that had high impacts to the growth of CNT forests. The parameters determining the drawability of the CNT forest were discussed. The drawable CNT forests were achieved in large areas by using both acetylene and ethylene processes. Processes for fabricating polymer–CNT composites were explored and developed. It was found that using a CNT yarn array as filler was an effective way to control the CNT distribution and content in composites and the best way to reinforce the polymer composite while keeping a high level of transparency of the composite. The reinforcement was significant. When using poly(methyl methacrylate) (PMMA) as the polymeric matrix, modulus and strength of the composite increased linearly with the increase of CNT content. Compared to the neat PMMA sheet, the -PMMA–CNT-yarn composite containing 17 wt% CNT had a 5-fold, 10-fold, and 8-fold improvement, respectively, in tensile strength, modulus, and toughness of the composite. Moreover, the composite had more than 40% transmittance at a CNT content of 19 wt%. Improving the properties of CNT yarns and/or increasing the content of CNTs could further improve mechanical properties of the polymer–CNT composite without disturbing its thermal properties. Calculations were also performed to evaluate the experimental results and predict the composites' properties. This program demonstrated that using a highly organized CNT assembly—such as CNT yarns—as filler is an efficient way to improve the properties of a polymeric composite while keeping the transparency of the composite. The technology developed in this program can be applied to other polymeric matrices.

2. INTRODUCTION

2.1 Background

Explosions release a large amount of energy in a very short time. Part of the energy is released as heat and part as shock waves that travel through the air and the ground. The shock wave (air blast) radiates at supersonic speed in all directions from the explosive source, which can propel blast-generated debris with great force. To buildings and vehicles nearby, the initial blast wave typically shatters windows and causes other damage to the building façade. In the second stage, the blast wave enters the building and exerts pressure on the structure. Air-blast pressures within a building can actually increase as the pressure waves reflect from surfaces and cause injuries to the occupants directly by means of either physical translation, ear, lung, and other organ damage, or debris from building elements and contents. Moreover, dynamic pressures occur somewhat later caused by the mass movement of the air itself.

The structural and other damage caused by an explosion is the building's response to the enormous amount of energy produced. This energy can be either resisted by massive elements that are strong or ductile enough to survive without failure or accepted in the form of partial damage to windows, façade and structural members. By balancing security and aesthetics, one can design various elements that will resist long enough to absorb a large amount of energy and then fail in a way that minimizes the risk of serious injury or death to the occupants. For blast protection, retrofitting concrete and masonry structures with fiber-reinforced polymer (FRP) composites has been successfully developed.[1] It is desired to increase the blast resistance of windows.

It is critical that the window structural elements be capable of deforming well beyond the elastic limit without experiencing structural collapse and be capable of very large plastic deformations without complete failure. This means that the materials used in the blast-resistant window should have high impact strength, be ductile enough to survive without failure, and have a certain amount of transparency. The study of FRP composites has overwhelmingly indicated that FRP and polymer retrofitting can significantly increase the blast resistance of a structure by increasing the structural strength and ductility plus reducing fragmentation.[1] Carbon nanotubes (CNTs) are one of the strongest fibers, and could be an excellent filler to increase the blast resistance of windows.

CNTs are very attractive candidates for diverse nanotechnological applications because of their structural characteristics and their extraordinary electrical and mechanical properties (tensile strength on the order of 100 GPa, stiffness *ca*.1000 GPa, and failure strain up to 0.4).[2,3] CNTs can react with various classes of compounds and be integrated into inorganic, organic and biological systems.[4] They demonstrate great potential for improving mechanical properties, especially fracture toughness of polymer nanocomposites.[5,6] Significant progress has been achieved recently in understanding the fundamental regularities of deformation processes of single macromolecules, single nanotubes, and nanocomposites,[7] and especially in solving the most difficult problem of stress transfer through the interface between the nanotubes and polymers.[8]

Reinforcement of CNT–polymer composites is influenced mainly by three factors: 1) dispersing the CNTs in the polymer matrix, 2) interfacial bonding between CNTs and polymer, and 3) aligning the CNTs in the polymer matrix. Until now, improvements in mechanical properties of the neat polymers by carbon nanotube incorporation remain modest compared to what should be expected from nanometer-scale reinforcement. The limiting factor in each application remains poor dispersion of nanofillers in the polymer matrix.

We were able to fabricate CNT–polymer nanocomposites without problems associated with CNT dispersion and alignment through the development of an innovative way to produce *transparent* CNT sheets.[9] The CNT sheets are drawn from nanotube forests In which CNTs are uniformly distributed and well aligned in each sheet. An as-drawn nanotube sheet is an unusual state of matter, a highly oriented aerogel that is self-supporting despite having an areal density of 1~3 $\mu g/cm^2$ and a volumetric density of 0.0015 g/cm^3. Transmittance of the densified, multiwalled CNT sheet was >85% for perpendicular polarization, >65% for parallel polarization between 400 nm and 2 μm, and >85% for unpolarized radiation between 1.5 and 10 μm. Also important for the applications, the measured gravimetric strength of the densified nanotube sheet was very high, 460 MPa/(g/cm^3). The CNT sheet is a free-standing sheet and can be placed on the surface of other materials and multi-stacked. Relevant for application to active materials and devices, these nanotube sheets applied to a plastic substrate can be severely bent repeatedly without significantly changing resistivity during the bending process. Introducing twist during sheet draw assembles CNTs into a yarn, in which CNTs are aligned at a curtain angle to the axis of yarn. CNT yarn has higher strength and modulus than CNT sheet.

2.2 Program Objectives

The goal of this project was to provide science and technology that enable the deployment of CNT assemblies that can be used to increase the blast resistance of windows, namely, using CNTs as filler to reinforce the transparent polymeric matrix. Since CNTs absorb visible light, uniformly dispersing CNTs into a polymer matrix causes the composite to lose transparency even with small CNT content. Therefore, this program was focused on developing processes to fabricate the CNTs, assemble them into well organized structures, and fabricate polymeric composites by using highly organized CNT assemblies.

The overall technical objectives of the program are to 1) optimize the method/process for synthesizing drawable CNT forests; 2) understand and improve the transformation of CNT forests into sheets and yarns; and 3) fabricate prototype CNT sheet- and yarn-reinforced polymer composites for blast-resistant applications.

2.3 Methods, Assumptions, and Procedures

The program was organized into three distinct but interrelated technical tasks, each aimed at achieving one of the above three program objectives. The three tasks were as follows:

Task 1: Synthesis of Drawable CNT Forests: This task investigated the effect of parameters (catalyst thin film, catalyst particle size, substrates, process temperature, etc.) on the formation of catalysts for CNT growth. The morphologies of catalysts were observed under various process

conditionsand the impact of process parameters on the drawability of the CNT forest was investigated. This task was intended to develop an effective manufacturing process to produce drawable CNT forests with nanotubes of high quality and long length. See Section 3.1 for further details.

Task 2: Assembly of CNT Sheet: This task utilized the results from Task 1 to understand the unusual forest topology that was drawable. The analysis and calculation were performed for us to further understand and improve the production processes. See Sections 3.2 and 3.3 for further details.

Task 3: CNT-Reinforced Transparent Polymer Composite: This task attempted to use black material, CNTs synthesized in Task 1 and assembled in Task 2, as fillers to reinforce a transparent polymeric matrix. The goal was to enhance the modulus, strength, and toughness of the composite while maintaining its transparency for use in windows. The processing–nanostructure–property relationships of the resultant CNT–polymer materials were explored and understood. We obtained the relationship of transparency and mechanical properties of the composite with the amount of CNTs in the polymer matrix, in the form of sheets, strips, or yarns. Calculations were performed to evaluate the processes and results. See Section 3.3 for further details.

The overall processes and procedures are shown in Figure 1. Detailed experimental procedures and results are described in Section 3. Results and Discussion.

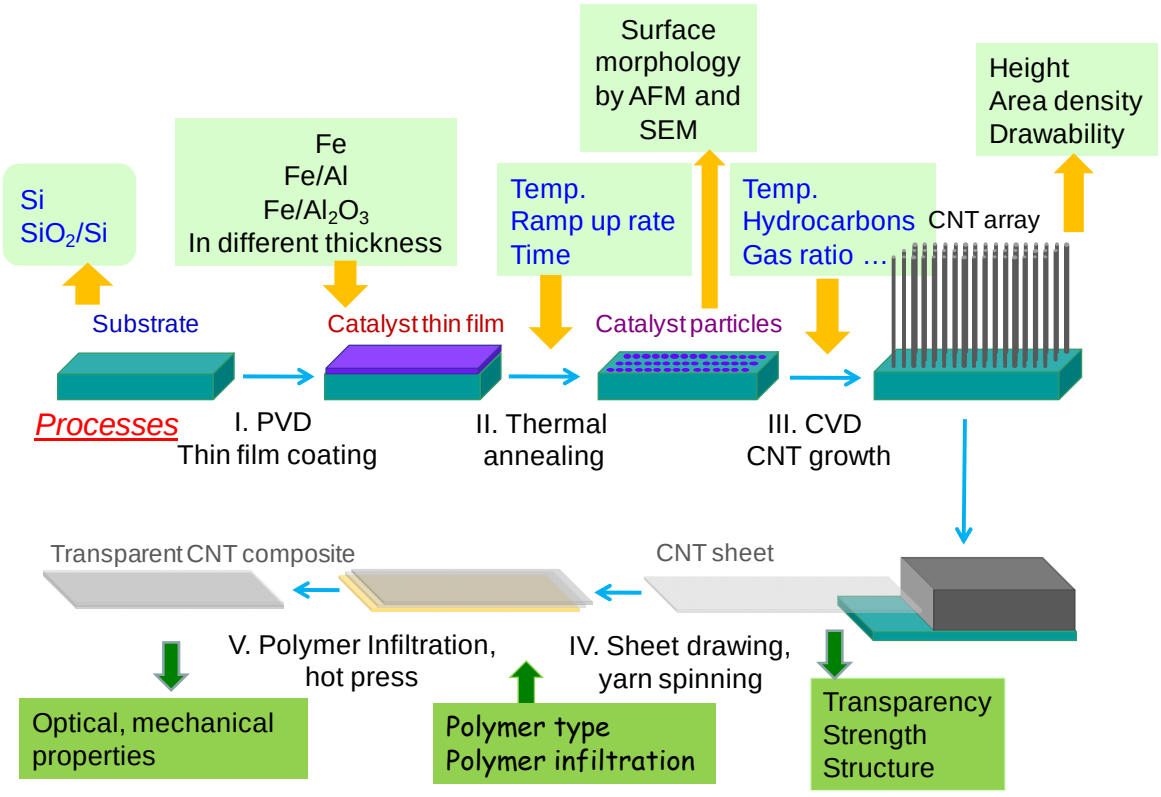

Figure 1. Illustration of the Processes and Parameters in Experimental Investigation

2.4 Program Team

A diverse and highly qualified team was assembled to address the technical challenges of the proposed program. The team members were faculty members of the Department of Industrial and Manufacturing Engineering at FAMU–FSU College of Engineering. Dr. Mei Zhang has extensive experience in the area of CNT assembly and led this program. She was responsible for the work on producing of CNT sheets and yarns, as well as nanotube-enhanced, transparent, polymeric composites. Dr. Richard Liang and Dr. Chuck Zhang have carried out research on CNTs and nanocomposite processing. Dr. Ben Wang led the effort for design/fabrication of windows from the nanotube assembly and lamination experiments.

3. RESULTS AND DISCUSSION

This Section is divided into three subsections corresponding to the three major tasks of this program. Section 3.1 focused on investigation on the effects of catalyst and process parameters on the growth of the special CNT forests. Section 3.2 discussed the impact of factors on drawability of CNT forests. Based on the results of Section 3.1 and 3.2, Section 3.3 demonstrated a successful process and improvement in properties of the CNT-reinforced polymeric composite.

3.1 Synthesis of Drawable Carbon Nanotube Forests

CNTs can be produced by many methods, including chemical vapor deposition (CVD), pulsed laser vaporization, plasma-enhanced CVD, and electric arc discharge. Among these synthetic methods, thermal CVD is paving the way toward the controlled synthesis of CNTs. Catalytic decomposition of hydrocarbons is a promising means to produce CNTs on a large scale.[1,10] In this program, catalytic CVD was used to synthesize CNTs.

Although the technology of CNT synthesis has continuously progressed over the past decade,[11–12] the ability to accurately control the diameter of CNTs and produce them with consistent quality remains a major technical challenge. Successfully synthesizing drawable CNT forests strongly depends on our understanding of the fundamental mechanisms of formation of drawable CNT forests and of CNTs. In this project, experiments were performed over a wide variety of parameters to determine the best attainable relationship.

CVD System

Our nanotube growth system (Fig. 2a) is a commercial CVD system with a three-zone furnace and a 5–in. quartz tube. The length of the heating zone is 16 in., with a uniform temperature range of ~11 in. Temperature and gas flow are controlled by computer interface. The increased dimension of the system dramatically boosts the throughput of forest growth. The CVD system was set up in our lab prior to the project's starting. After systematic trial-and-error tuning of reaction conditions, we have successfully grown drawable forests at large scale using this system. Figure 2b shows the schematic setup of the CVD process for CNT growth. Typically, CNT forests were synthesized by atmospheric pressure CVD using 100 molar percent acetylene (C_2H_2) in argon (Ar) at ~700 °C, at a total flow rate of 5000 sccm for 10 minutes. With this system, we are able to produce drawable CNT forests with dimensions of 20 cm x 12 cm. We also successfully switched the carrier gas from helium (He) to Ar for the synthesis of drawable forests during the project period, which lowered the CNT fabrication cost.

Substrate and Catalyst

The substrates are polished (100) silicon (Si) wafers (*p*-type, 725 μm thickness, Silicon Quest International) and Si wafers with a 500-nm layer of silicon dioxide (SiO_2) on top. Iron (Fe) was selected as the catalyst for CNT growth. The catalyst Fe and a buffer layer of aluminum (Al) or alumina (Al_2O_3) are deposited on the Si wafer by electron beam (e-beam) evaporation. A film of Fe catalyst and buffer-layer Al_2O_3 is deposited by e-beam evaporation in a single pump-down cycle. The Al_2O_3 is deposited by direct evaporation from a crucible of high-purity crystals, rather

[1]. H. J. Jeong, et al. *J. Phys. Chem.* **B 108**, 17695 (2004).

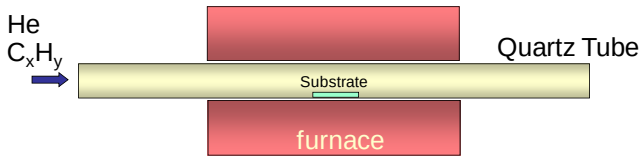

(a) (b)

Figure 2. (a) CVD System for Synthesis of CNT Forests. (b) Schematic Setup of the CVD Process for CNT Growth

than by evaporation of Al with a slight background pressure of oxygen (O_2), or by other methods such as spin-coating of a sol–gel precursor. To prepare Al/Fe, the film of Al is deposited first, and then oxidized naturally in air before depositing the Fe film. After catalyst deposition, no further cleaning or dedicated oxidation was performed prior to nanotube growth. A variety of catalysts were used in this work (Table 2). The thicknesses of both buffer layer and catalyst were changed to investigate their effects on CNT forest growth. For the investigation of synthesis conditions, substrates were 5-mm or 10-mm square coupons, and several substrates with different types of catalysts were placed adjacently inside the furnace during CVD processing. A piece of Si wafer of a size up to 20 cm x12 cm was used to grow uniform CNT forests for drawing CNT sheets or spinning CNT yarns.

Characterization

The thin catalyst film segregated into small islands during heat treatment. After heat treatment, the samples were observed by scanning electronic microscopy (SEM), LEO 1530 VP (JEOL JSM-7401F), and evaluated by atomic force microscopy (AFM). The SEM was operated in high-vacuum mode at 10 keV. AFM measurements were performed in tapping mode at ambient conditions. Root-mean-square (rms) roughness was measured over the whole area.

The height of the CNT forest was measured using a 100X optical microscope. The structure of the CNT forest was observed by SEM. The surface morphology and catalyst nanoparticle sizes and distributions on the silicon substrate after CNT synthesis were also investigated by SEM and AFM. These are important factors because they determine the CNT diameter and distribution (density of CNT forest).

3.1.1 Catalyst Morphology

The general CNT growth mechanism can be explained by the vapor–liquid–solid model, which involves the dissociation of hydrocarbon molecules by transition-metal nanoparticles, and dissolution and supersaturation of carbon atoms in the catalyst particles. Among many factors that affect the growth of CNTs, the catalyst is key. Catalysts act as “seeds” for CNT growth. They are placed in contact with a gaseous carbon or hydrocarbon source that deposits carbon on the surface of the catalyst particle. The deposited carbon atoms then rapidly diffuse toward the

base of the nanotube, which is grown from the surface of a catalyst particle. The diameter of the nanotubes is closely related with the topography of the catalyst particles. Namely, the growth of CNTs is catalytically controlled; the catalyst plays an imperative role in determining the outcome. The key to catalytic growth of CNTs is in the processes that occur at the surface of or within the catalytic particle, because the catalyst particle is responsible for breaking bonds, adsorbing carbon at its surface, and then diffusing carbon through or around an interface where the carbon reforms in graphitic planes. The properties of the catalyst can, therefore, determine the rate of each of these steps as well as the degree of crystalline perfection and geometric structure of the resulting CNTs. In our process, we chose iron as the catalyst because iron is known to be very active in its ability to break and reform carbon–carbon bonds.

We used thin-film technology to form catalyst particles. Physical vapor deposition of a thin film of catalyst on the substrate was achieved by, e-beam evaporation. The substrates were silicon with or without buffer layers. The roughness of the substrate surface was nanoscale, which is helpful to form nanoscale catalyst particles distributed uniformly.

A very uniform iron film few nanometers thick is placedon the substrate. To grow CNTs from a thin-film catalyst, the film must be sintered into islands or discrete nanoparticles. Since nanotubes are of such small dimensions, the size and uniformity of the nanoparticles is exquisitely important.

In our CNT synthesis, process II thermal annealing and process III CVD CNT growth (Fig. 1) are continuous processes, so there is no substrate (catalysts) treatment before the CVD process. Instead, the catalyst particles for CNT growth are formed during temperature ramp up and before the carbon source gas flows into the reactor. To better understand the impact of catalysts, we tried to anneal the substrate and to apply substrate surface morphology analysis to see what formed on the substrate before CNT growth .

Experimental conditions for catalyst morphology investigation are summarized in Table 1. To simulate the CNT growth conditions, thermal annealing was performed at 650 °C, 680 °C, 710 °C, 730 °C, 750 °C, and 780 °C using the same temperature ramp-up rate and annealing time in an Ar environment. Temperature ramp-up-time experiments are to investigate the size of catalyst particles, and the annealing time is studied to evaluate the effect of remaining at high temperature on the catalyst particles. For each investigation, more than 10 kinds of substrates

Table 1. Conditions for Catalyst Morphology Investigation

Carrier gas	Ar	5000 sccm
	H_2	500 sccm
Hydrocarbon gas	C_2H_2	0 sccm
	C_2H_4	0 sccm
Annealing temperature		650, 680, 710, 730, 750, 780 ºC
Temperature ramp time		5, 17, 30 min
Annealing time		2, 12, 30 min
Reaction pressure		Atmospheric pressure
Substrate buffer layer		SiO_2, Al, Al_2O_3
Thickness of Al, Al_2O_3 and Fe		0 ~ 8 nm

were used to explore different thickness of catalyst film or different buffer layers. Substrates used in investigating catalyst morphology are listed in Table 2. Figure 3a illustrates the structure of the substrate and Figure 3b shows samples for each thermal treatment condition.

Table 2. Sample Number and Thickness of the Catalyst Film and Buffer Layers

Sample name	Thickness (nm)			Sample name	Thickness (nm)		
	Fe	**Al**	**Al_2O_3**		**Fe**	**Al**	**Al_2O_3**
Cat 1	1.2			Cat 19	1.2		
Cat 2	4.5			Cat 20	1.1		
Cat 3	3.0			Cat 21	1.3	1.0	
Cat 4	4.0			Cat 22	1.2	1.4	
Cat 5	6.5			Cat 23	1.5	2.0	
Cat 6	2.5			Cat 24	2.0	2.2	
Cat 7	5.0			Cat 25	1.2		8.0
Cat 10	2.0			Cat 26	1.2		2.8
Cat 11	1.8			Cat 27	1.2		2.0
Cat 12	1.1			Cat 28	1.2		
Cat 13	0.8			Cat 29	0.8		
Cat 14	1.5		>10	Cat 30	1.2		15
Cat 15	1.2	1.0		Cat 31	1.2		
Cat 16	0.7			Cat 32	0.8		8.0
Cat 17	1.0			Cat 33	0.8		2.8
Cat 18	1.4			Cat 34	0.8		2.0

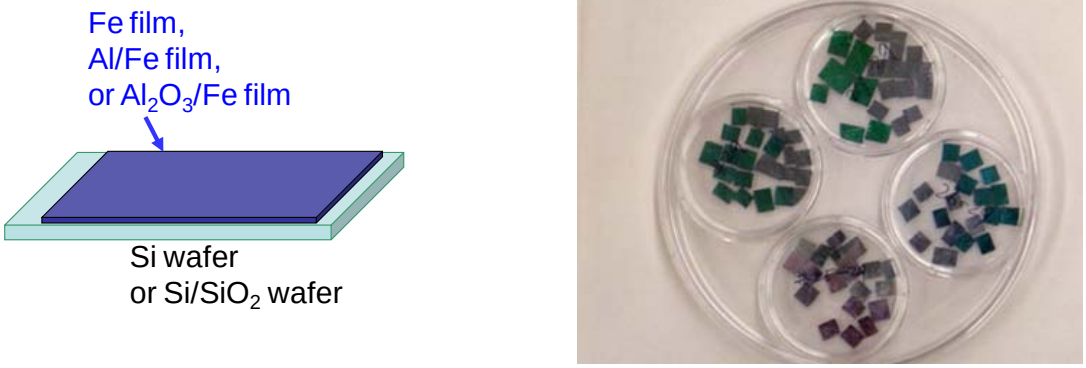

(a) (b)

Figure 3. Samples for Catalyst Morphology Investigation. (a) Illustration of the Substrate Structure. Catalyst (Fe) Film and Buffer (Al or Al_2O_3) Layer are Evaporated on a Si Wafer or a Si Wafer With a Thin SiO_2 Layer. (b) Samples with Different Fe Thickness, Buffer Layer, or Combinations Were Used for Each Thermal Annealing Experiment

Catalyst Film Thickness

An iron film few nanometer thick, deposited on a polished Si wafer by e-beam evaporation, is very uniform and smooth. AFM observation shows that the surface roughness is within 1 nm. During temperature ramp-up to the temperature for CNT growth, the thin-film catalyst is sintered into islands or discrete nanoparticles.

Figures 4 and 5 show AFM images of Fe films 3, 4, 4.5, 5 and 6.5 nm thickafter thermal treatment at 650°C and 710°C, respectively. The surface roughness was obtained by AFM profile scanning. The lines in images show the scan traces of the surface roughness. It is obvious that surface roughness increases with thickness of the Fe film. The thicker Fe films form big grains on the substrate surface, which is not satisfactory for CNT growth.

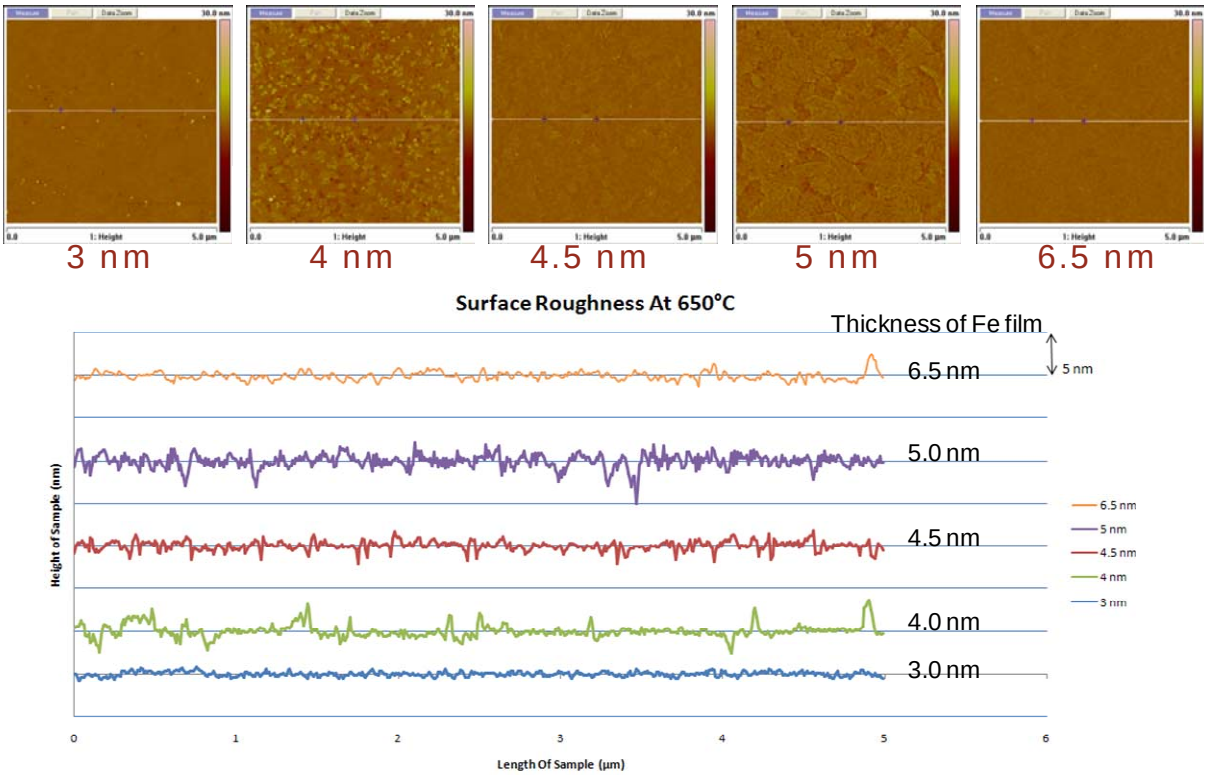

Figure 4. AFM Results Show the Effect of Fe Film Thickness at 650 °C

It is clear that the size of the catalyst particles is ultimately determined by the thickness of the film, as are the wetting properties of the catalyst and substrate materials, but the method of catalyst preparation and pretreatment also contributes. Forming smaller catalyst particles with high density on the substrate will benefit the growth of the drawable CNT forest. The CNT growth demonstrates that Fe films thicker than 4 nm produce forests that are undrawable (Section 3.1.2).

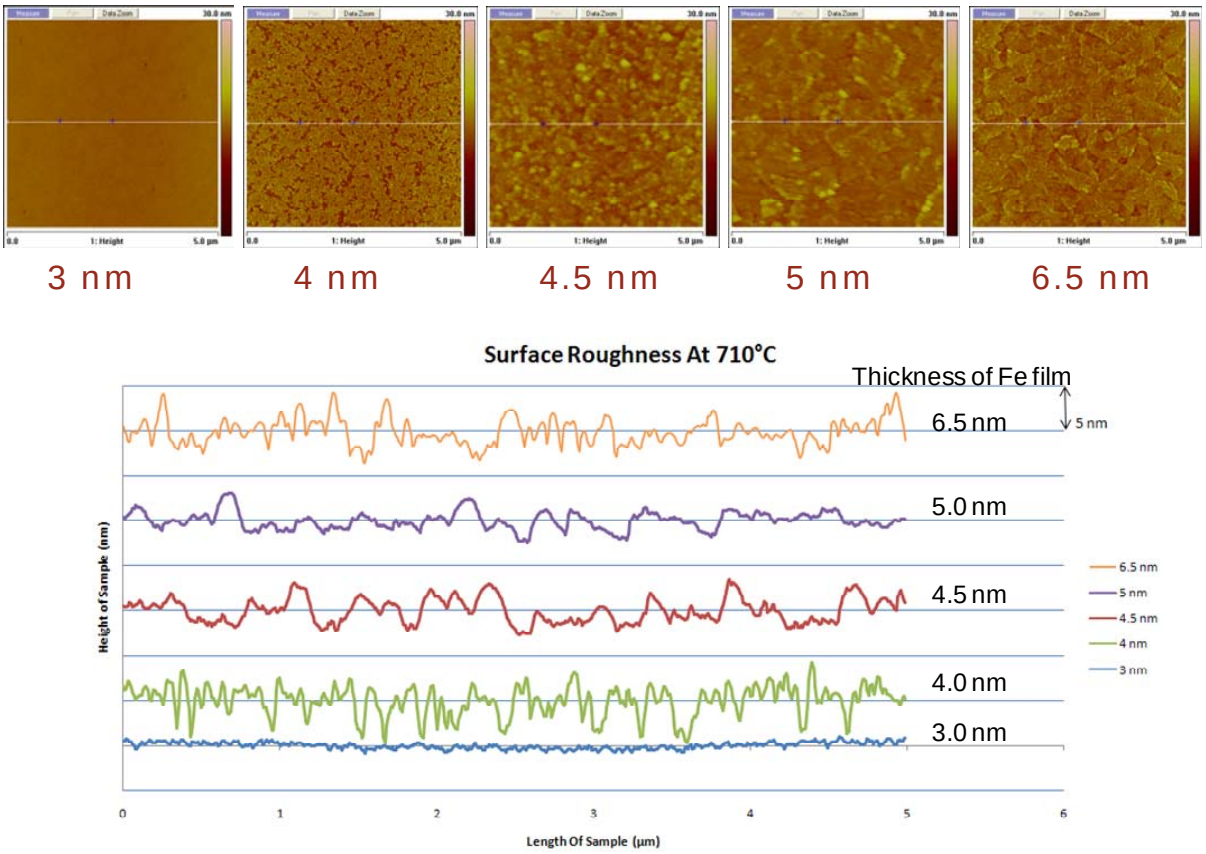

Figure 5. AFM Results Show the Effect of Fe Film Thickness at 710 °C (The Frame Size of the AFM Images is 5 µm)

Substrate

A nanotube grows away from the catalyst particle by deposition of carbon in the contact region between the catalyst particle and the already formed tubule segment. Compared to the top-growth mechanism, bottom growth allows for better connections between CNTs and the substrate. For drawing CNTs from the forest, bottom growth is preferred because it gives better control of the density and the structures of the forest, and the sheets and yarns retain high purity because the catalysts bind strongly with the substrate. Top or bottom growth is controlled by choosing a suitable catalyst type and support material. Proper selection of the support material beneath the catalysts is critical for CNT growth. In most cases, we used bare Si wafers and Si wafers with a top oxidized layer (Si/SiO_2). Figure 6 shows the surface morphology of catalysts on Si and Si/SiO_2 substrates after, thermal annealing for 2 min at 710 °C. The surface of the Si/SiO_2 substrate is rougher than that of the Si substrate. However, the morphologies of the catalyst are similar for catalyst films thicker than 4 nm.

Catalyst morphology in an alumina buffer layer appears to be very different from that without the buffer layer. The surfaces come out much smoother and the particles size is much smaller after the same thermal treatments. No big particles formed on substrate before and after CNTs growth and the size of the roots of the tubes are much smaller. The alumina under layer is necessary for the synthesis of smaller-diameter tubes.

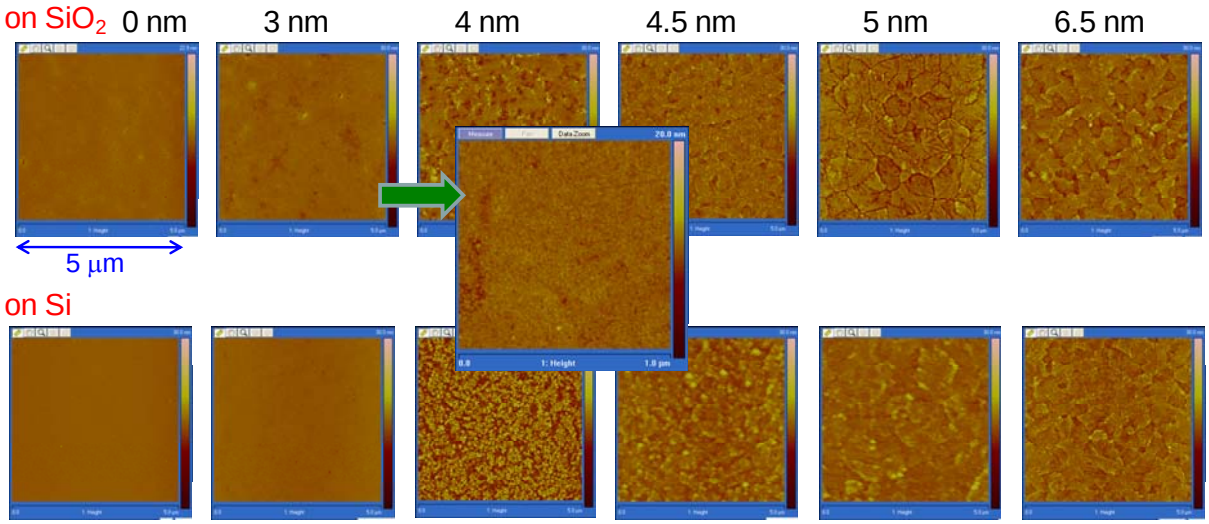

Figure 6. AFM Images of the Surface Morphology of Fe Films on Si or Si/SiO_2 Substrates (Frame Size 5 μm)

The size and the distribution of the catalyst on the substrate can be optimized by adjusting the roughness of the surface and the thickness of the catalyst thin film. This thin-film technique is suitable for harvesting the same type nanotubes on a large scale.

Temperature Ramp-up Rate

There are no treatments to the substrate after catalyst films are coated, so the catalyst particles are formed during temperature ramp up and before CNT growth. The purpose of this experiment is to investigate how the formation of catalyst particles and its activity depend on the ramp-up time. The ramp-up time was set at 17 to 33 min for the temperature ramp from room temperature to 710 °C because 17 min is the time of the maximum ramp-up rate of the furnace, 40 °C/min. In experiments, we also heated the reactor up to 710 °C and kept that temperature, then pushed the substrates into the reactor to subject the substrates to the highest heating rate attainable in our setup, ~150 °C/min. Figure 7 shows AFM images of the substrate surface after heat treatment. At the high heating rate, thermal shock could lead to the formation of smaller catalyst islands and higher density of catalysts on substrate. However, the results displayed in Figure 7 do not show a significant difference. Thus, in the growth of CNT forests, we can use the high ramp-up rate to shorten the process time and save time and energy.

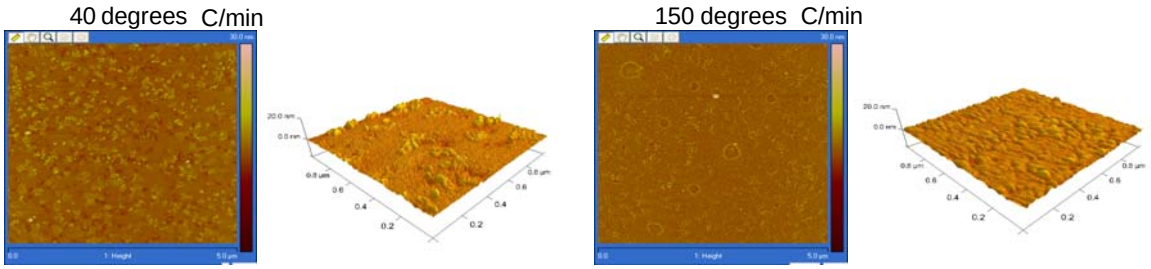

Figure 7. Effect of Temperature Ramp-up Rate on the Surface Morphology Annealing Time

In the CNT growth process, the heating rate was usually lowered by the system as the temperature approached the set point, to prevent overshooting the temperature limit. This caused the substrate to stay a longer time at the process temperature before CNTs start to grow. The time after the substrate reaches the process temperature and before CNT growth starts is called the *annealing time*. Annealing time effects were investigated on Fe/Si samples at a process temperature of 730 °C. Figure 8 shows the surface morphology of the catalyst after annealing in Ar at 730 °C for 2 min, 12 min, and 30 min. The morphologies of catalysts layers among the samples after different annealing times look very similar after 2 min, 12 min or 30 min of thermal treatment. This means that an initial annealing process is not necessary for the synthesis of drawable forests.

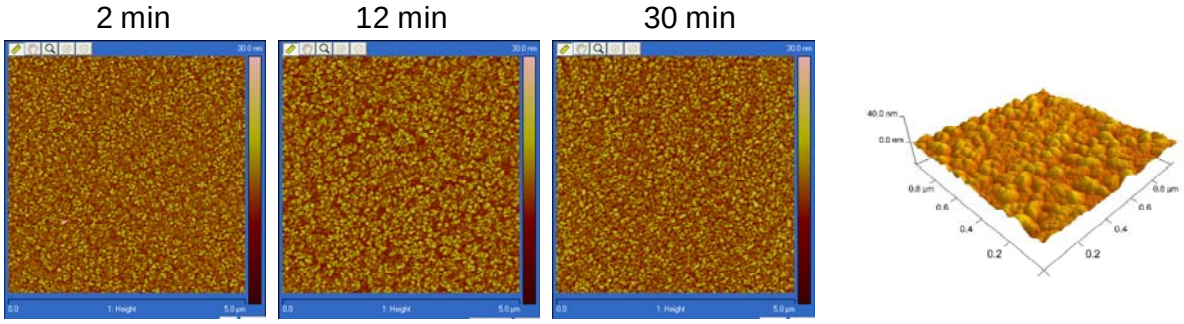

Figure 8. Effect of Annealing Time

Process Temperature

Process temperature is important—decomposition of hydrocarbon gases and gas–catalyst reactions are temperature driven. To the catalysts, a higher process temperature means longer thermal treatment time. It is clear that the annealing time and ramp-up rate do not have significant effects on catalyst morphology (Figs. 7 and 8)—the catalyst has similar morphology at process temperatures from 650 °C to 750 °C. Figures 9 and 10 show the surface roughness of substrates with 3- and 4-nm catalyst thickness, respectively. It appears that the catalyst film transfers into particles before the system temperature reaches 650 °C. The size of catalyst particles depends on the initial thickness of the deposited catalyst film.

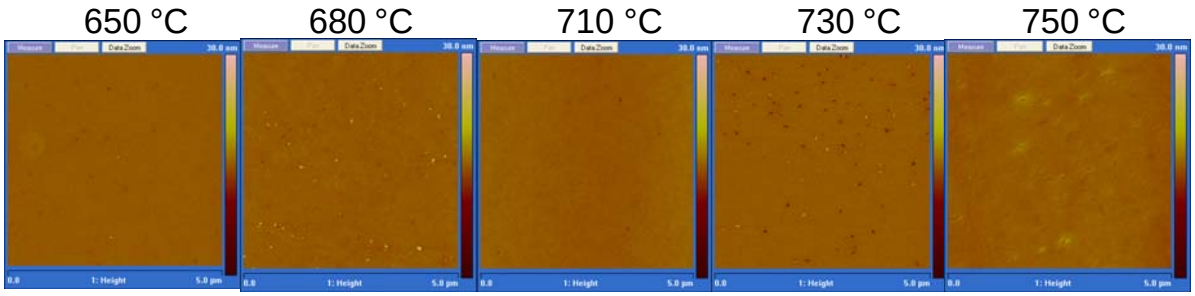

Figure 9a. Effect of Annealing Temperature on a 3-nm Fe Film on Si

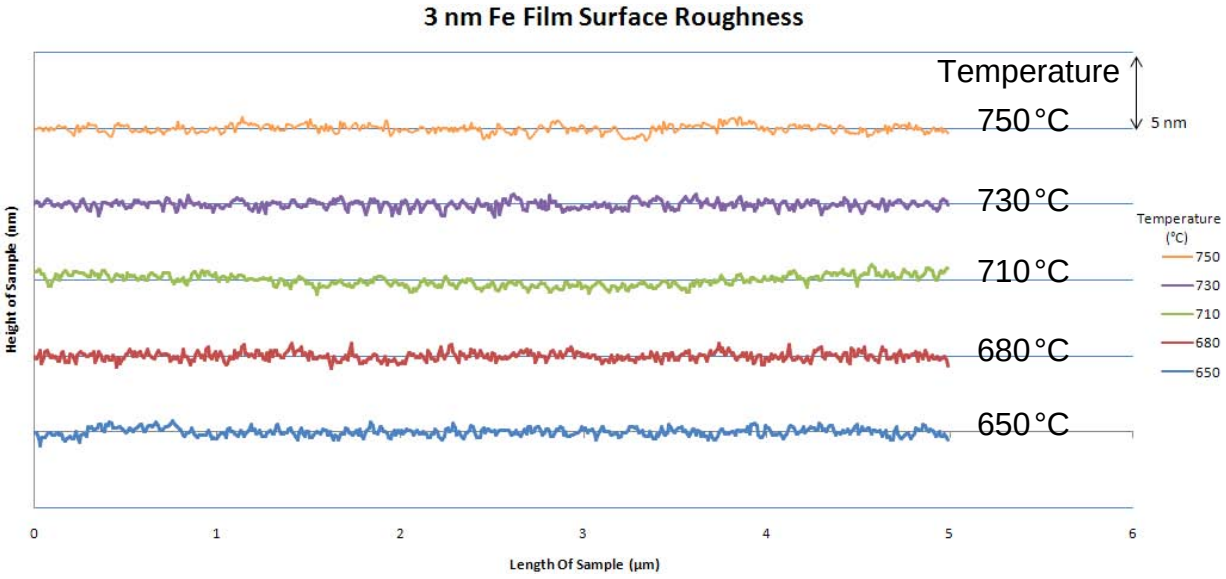

Figure 9b. AFM Results Showing the Effect of the Annealing Temperature (3-nm Fe Film on Si)

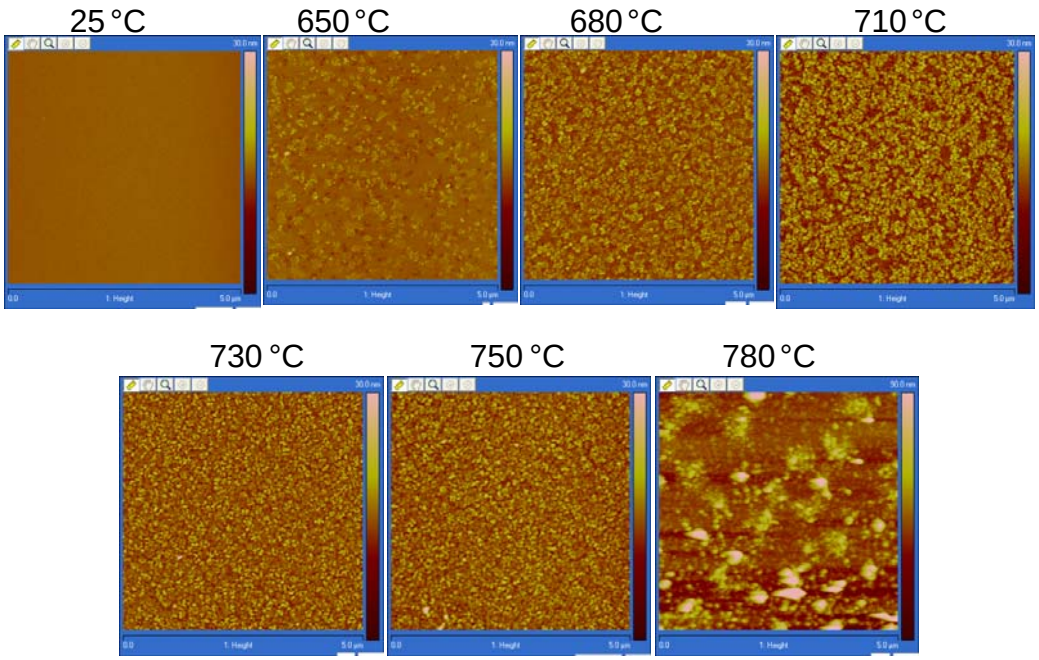

Figure 10a. Effect of Annealing Temperature on a 4-nm Fe Film on Si

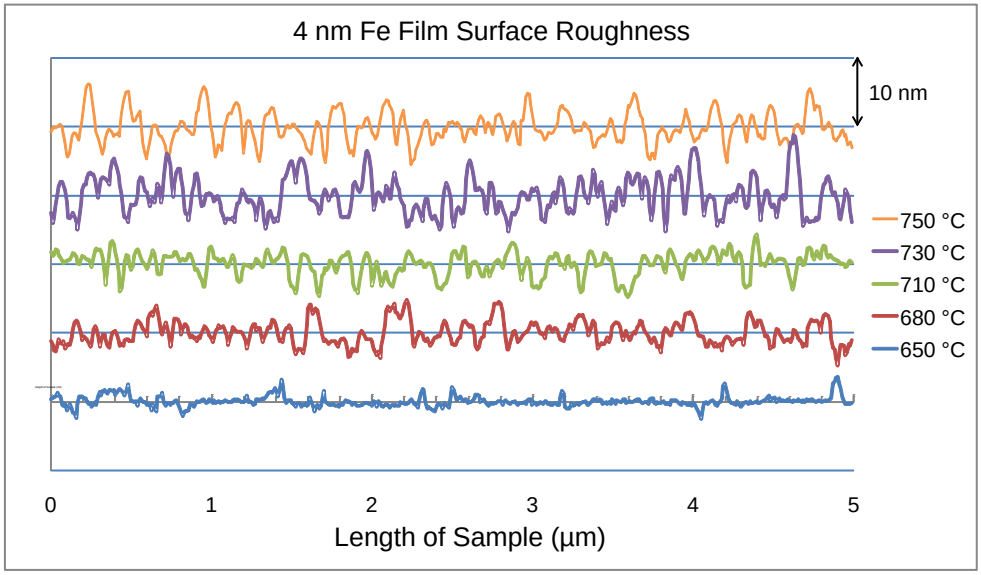

Figure 10b. Effect of the Annealing Temperature (4-nm Fe Film on Si)

3.1.2 Carbon Nanotube Synthesis

CNT forest growth is performed in a conventional, three-zone, atmospheric–pressure, quartz-tube furnace, with a 12-cm inner diameter and a 40-cm-long heating zone. Flows of Ar (99.999%), C_2H_2 (99.6%), ethylene (C_2H_4, 99.95%), and hydrogen (H_2, 99.999%) are regulated by a mass flow controller. After the substrates are loaded into the tube, the chamber is pumped

and filled with Ar to atmospheric pressure. Next, the furnace temperature is ramped linearly to the set point temperature with a flow of 5000 sccm Ar. Then the reactant gases are introduced during a growth period of typically 10 min. A constant 5000 sccm Ar flow is maintained to displace the growth gases from the quartz tube and during furnace cool-down.

The synthesis of CNT forests is a key step for solid-state fabrication of CNT sheets and yarns. Processability and the properties of resulting sheets and yarns strongly depend on nanotube length and morphologies of nanotubes in the forests. Research next focused on optimizing the process and improving the quality of CNTs, to reduce the number of defects in and better control the diameters of the CNTs. Both would significantly improve the mechanical properties of the CNTs as well as the sheets and yarns from them. The conditions investigated are total gas flow, ratio of Ar to hydrocarbon in the gas phase, reaction temperature, temperature ramp-up time, and catalysts. The conditions for CNT synthesis are summarized in Table 3. Growing uniform forests on a big area is also important for making CNT sheets and yarns. Several experiments were carried out on big substrate coupons. As shown in Figure 11, we achieved uniform CNT growth on a Si wafer 20 cm x 12 cm, the biggest size can be used in the CVD system. We also grew a CNT forest more than 1 mm high (Fig. 11b). Based on SEM and thermaogravimetric measurements, purity of the CNTs was very high (more than 99% carbon in the form of CNTs) with no observed carbon particles.

Table 3. Conditions for CNT Growth

Carrier gas	Ar H_2	5000 sccm 500 sccm
Hydrocarbon gas	C_2H_2 C_2H_4	90 ~ 300 sccm 90 ~ 300 sccm
Reaction temperature		680 ~ 780 ºC
Temperature ramp time		17 ~ 33 min
Reaction time		5–30 min
Reaction pressure		Atmospheric pressure
Substrate buffer layer		SiO_2, Al, Al_2O_3
Thickness of Al, Al_2O_3, and Fe		1 ~ 10 nm

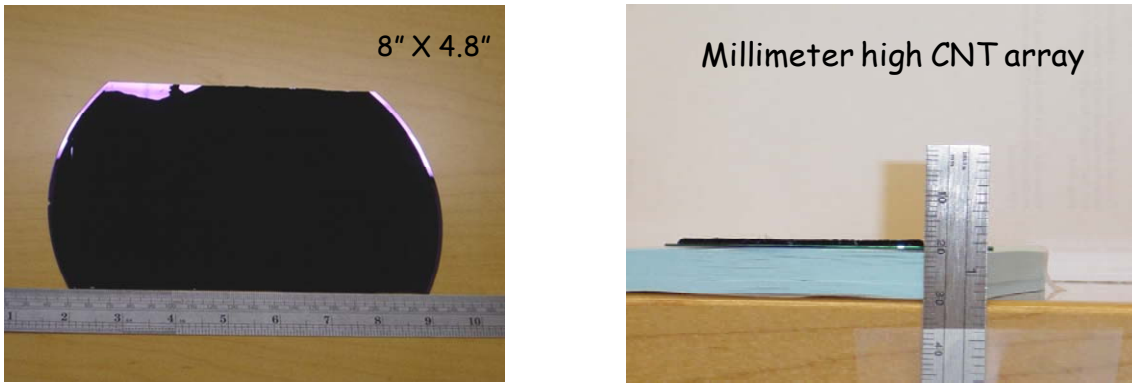

(a) (b)

Figure 11. (a) Uniform CNT Forest Grown on a 20-cm x 12-cm Silicon Substrate. (b) Image of the Side View of a Forest More Than a Millimeter High

Effect of Catalyst Film Thickness

CNT growth strongly depends on the catalysts. As shown in Figures 4 and 5, in Fe films more than 4 nm thick the Fe film changed into grains of sizes unsuitable for CNT growth. The CNT growth results shown in Figure 12 are consistent with the observation of the catalyst morphologies in Figs. 4 and 5. Different thicknesses of Fe/Al and Fe/Al_2O_3 catalysts give very different growth rates and catalyst lifetimes of under the same CVD conditions. It is clear that synergy between the metal catalyst and the supporting material is critical for an efficient and high-yield CVD growth process. For synthesizing drawable CNT forests, the catalyst thin film needs to be thinner than 3 nm. SiO_2 on the substrate seems to have no big impact no CNT growth.

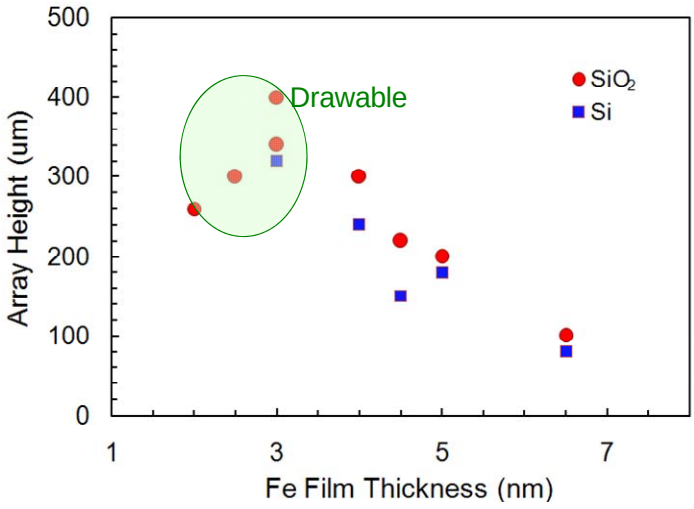

Figure 12. Dependence of CNT Forest Height on the Thickness of Fe Films

Effect of Process Temperature

Temperature influences the growth of forest because the activity of the catalysts and gas discomposition rates are strongly related with temperature. In this program, we explored the

temperature range from 690 °C to 745 °C. Catalysts A and B were formed from e-beam-evaporated Fe films 2 nm and 3 nm thick, respectively. The hydrocarbon gas was C_2H_2 and the process time was 10 min. As shown in Figure 13, the height of the forest increases as process temperature increases for both kinds of catalyst. However, the drawability of the forests differs. Drawable forests were obtained when the process temperature was between 710 °C and 720 °C. In Figure 14, a photograph shows a CNT sheet drawn out of a CNT forest and the SEM image gives the structure of the CNT sheet.

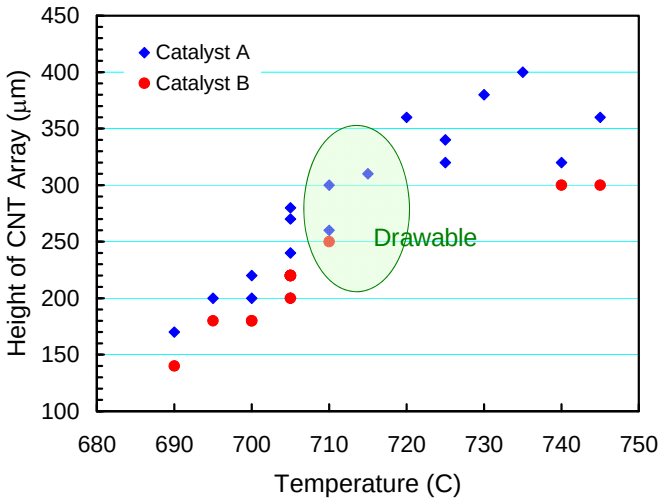

Figure 13. Temperature Dependence of the Forest Height

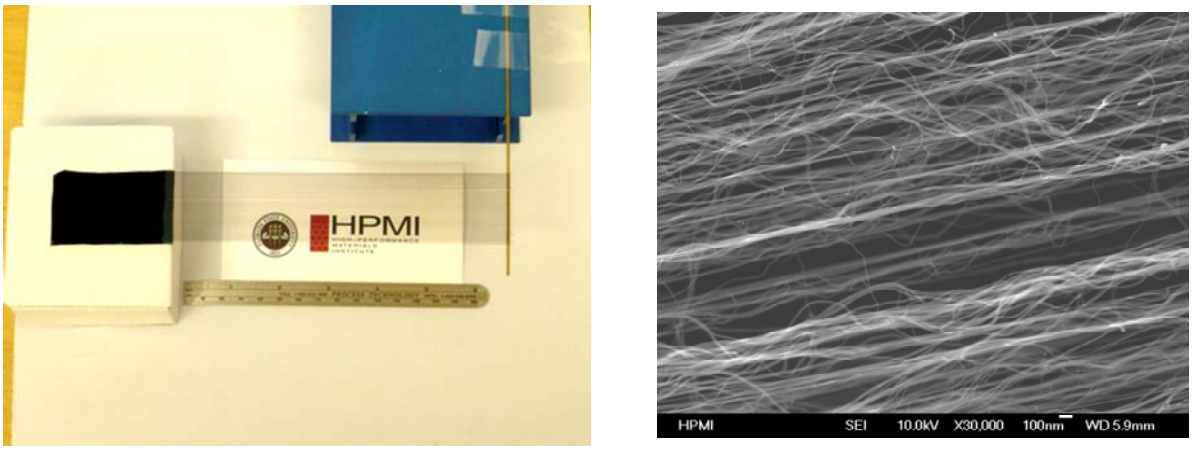

(a) (b)

Figure 14. (a) Optical Image of a CNT Sheet Drawn from a CNT Forest and (b) SEM Image of Aligned CNTs in the Sheet

3.2 Assembly of Carbon Nanotube Sheet

Most types of CNT forests are either unsuitable for drawing or produce weak sheets or yarns. The outstanding drawability of our forests is due to the unique structural nature of the forest. Nanotubes in the forest undergo intermittent bundling, meaning that an individual nanotube forms small bundles with a small group of neighboring nanotubes at one location along the forest height and with other small group of neighboring nanotubes at other locations along the forest height. Experimentally, we understood that the transition from drawable to non-drawable or difficultly drawable forests could be caused by relatively minor changes in the reaction conditions used for nanotube forest growth. Even changing the furnace size and type used for growing can dramatically change the drawability of forests and the ease of drawing forests. Combining with the experimental results, we performed analyses in the drawability of the forest. We believe the drawability of the forest depends on the length of the tubes, the purity of the forest, the density of the forest, and the structures in the forest. Among our CNT forests, the length and the purity are not significant factors. In this research, we paid more attention to the density of the forests. Since the CNTs in a forest have almost the same length, the volume density of the forest is directly related to its area density. As shown in Figure 15, drawability is a function of the area density of the forest. If the area density is very low, CNTs will lie on the substrate randomly. CNTs can grow in the out-of-plane direction and form a forest when its area density exceeds a threshold value. If the forest has very high density, the CNTs in the forest will form big bundles and the forest will not be drawable. A drawable forest should have a proper area density and structures.

3.2.1 Drawability of the Forest

We believe that purity of the tubes, the height of the forest, the morphology of the forest—especially the 3D structure by self-assembly during CVD processing—and the area density of the tubes are the main factors determining the drawability of the forest. Here, area density (number of tubes per square centimeter) plays an important role. Drawable forests must have area density

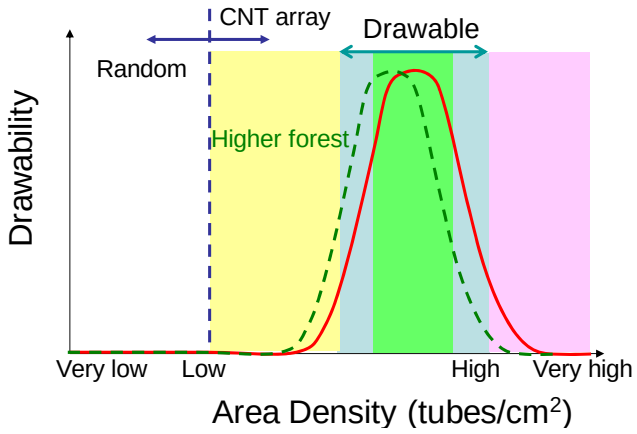

Figure 15. Diagraph Showing the Relationship of the Drawability of a Forest to Its Area Density

high enough for CNTs to form interactions in the forest. The required area density of the forest is related with the diameter of the tubes. Experimentally, the area density of the forest is calculated from counting the root of the tubes on the substrate after removing the forest on it. Figure 16 shows the surface of substrates after removal of forests made by the C_2H_2 process. Each round dot in the images is the root of a nanotube. As marked in Figure 16, four SEM images show the

CNT roots from drawable to undrawable forests. The drawable forest has higher CNT area density. Figure 16 also demonstrates that CNT growth strongly depends on the thickness of the catalyst films. The dependence of area density of CNT forests on the thickness of catalyst films

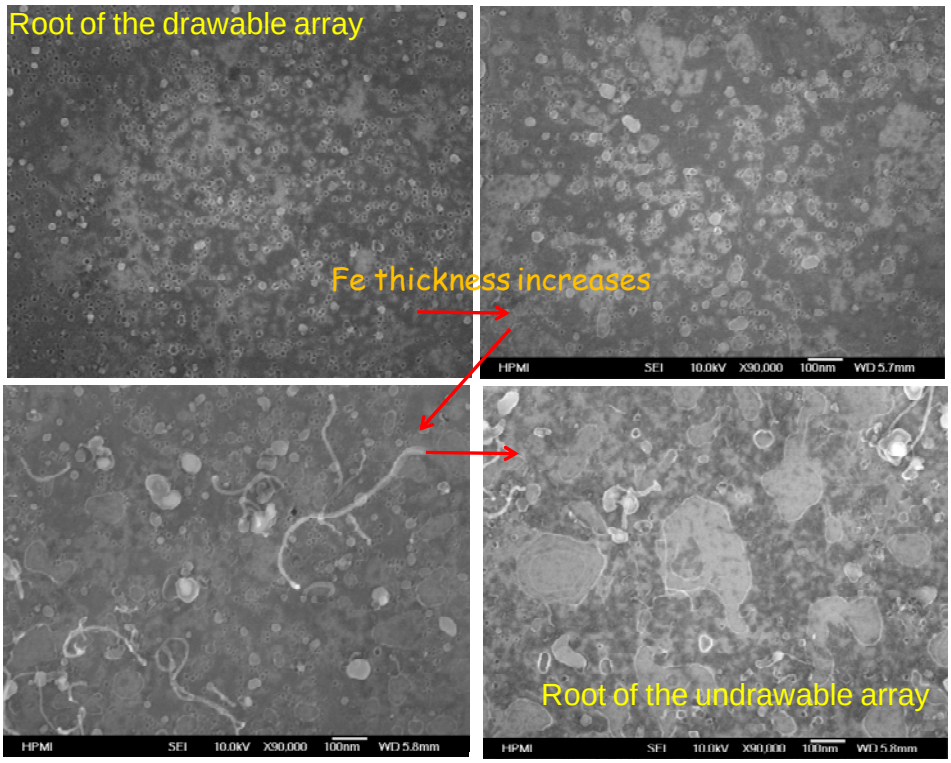

Figure 16. SEM Images of Substrate Surfaces after Removal of CNT Forests Made by the C_2H_2 Process

is plotted in Figure 17. The area density of an undrawable forest is ~10^{10}/cm^2, and the area density of well drawable forests is close to 10^{11}/cm^2. It is clear that thick catalyst films lead to smaller amounts of active catalysts (also see Figs. 4 and 5). Figure 18 illustrates typical surfaces of substrates after removal of forests made by the C_2H_4 process. The image in Figure 18 is from a drawable forest. However, the drawability is not as good as that produced by C_2H_2 process. Comparing Figure 18 with Figure 16, we can see that the size of the tubes is smaller, but the area density is still too low for a drawing process.

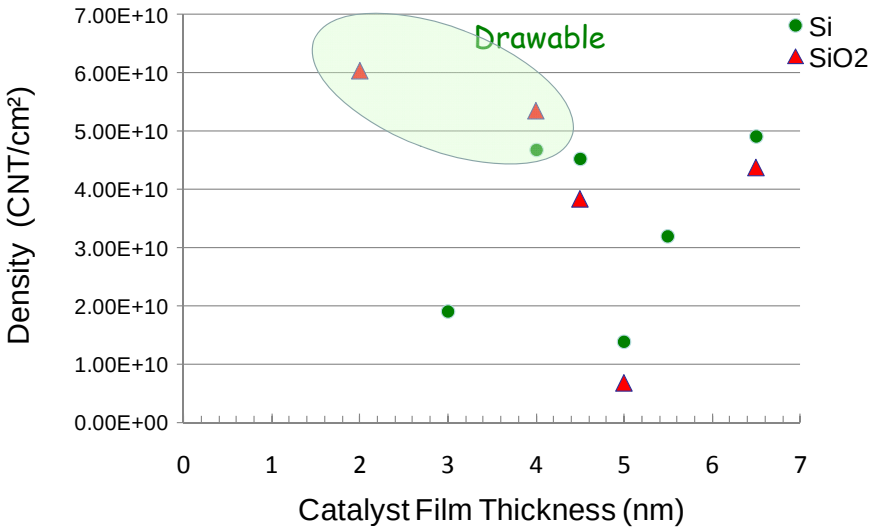

Figure 17. Effect of Catalyst Film Thickness on Area Density of CNT Forests Made by the C_2H_2 Process

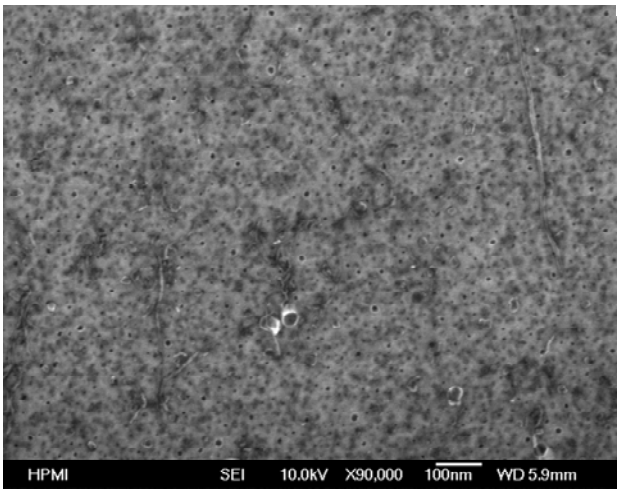

Figure 18. SEM Image of a Substrate Surface after Removal of a CNT Forest Made by the C_2H_4 Process

CNT forests grew well on both substrates, with/without a pre-annealing process. It is clear that the area density of the tubes has no direct relationship with the pre-annealing process. Keeping catalysts active is the key to increasing the area density of CNTs.

3.2.2 Coverage of Carbon Nanotubes on Substrate

We understand that the drawability of forests depends on the area density of CNTs on the substrate. The area density can be described by the percent coverage of CNTs on substrate. Undrawable forests result from low CNT coverage, which leads to inadequate connectivity between CNTs. Considering the interactions of the CNTs in the forest, area density of the CNTs is not a unique parameter that determines the drawability of the forest, which is also related to the diameter of the tubes. A drawable forest formed by smaller-diameter CNTs needs higher area

density than one populated with bigger-diameter tubes. Therefore, the coverage of the tubes on substrate is a better indicator to evaluate the drawability of the forest.

Experimentally, the coverage of 10-nm-diameter CNTs in a highly drawable forest is ~15%. Figure 19 is an illustration of the CNT coverage. Since a CNT has a circular cross-section, the area ratio (ratio of total area of CNTs to the area of forest covered on the substrate) is 78.5% when the CNTs are highly packed into a crystal structure, that is, complete coverage on the

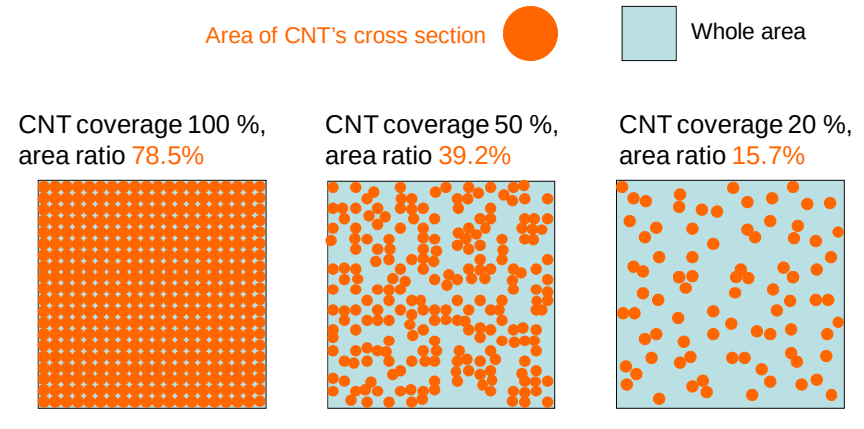

	CNT Area Density (/cm2)			
CNT coverage	100%	50%	20%	15%
CNT Diameter (nm)				
1	1.0E+14	5.0E+13	2.0E+13	1.5E+13
2	2.5E+13	1.3E+13	5.0E+12	3.8E+12
3	1.1E+13	5.6E+12	2.2E+12	1.7E+12
4	6.3E+12	3.1E+12	1.3E+12	9.4E+11
5	4.0E+12	2.0E+12	8.0E+11	6.0E+11
6	2.8E+12	1.4E+12	5.6E+11	4.2E+11
7	2.0E+12	1.0E+12	4.1E+11	3.1E+11
8	1.6E+12	7.8E+11	3.1E+11	2.3E+11
9	1.2E+12	6.2E+11	2.5E+11	1.9E+11
10	1.0E+12	5.0E+11	2.0E+11	1.5E+11
11	8.3E+11	4.1E+11	1.7E+11	1.2E+11
12	6.9E+11	3.5E+11	1.4E+11	1.0E+11
13	5.9E+11	3.0E+11	1.2E+11	8.9E+10
14	5.1E+11	2.6E+11	1.0E+11	7.7E+10
15	4.4E+11	2.2E+11	8.9E+10	6.7E+10

Figure 19. The Area Density of CNTs Depends on the Diameter of the Tubes

substrate. Obviously, full coverage is not only hard to produce experimentally, but it is also not drawable. Drawable forests usually have 10%~20% CNT coverage. Figure 19 shows that the CNTs form small bundles in the forest and those small bundles are connected by individual tubes or bundles (Fig. 14b). Based on the coverage, the relationship of the area density to the diameter

of the tubes is listed in Figure 19. More CNTs are needed to improve the drawability of the forest if the tubes are thinner.

Generally, the diameter of the CNT depends upon the size of the catalyst particle. In our case, as mentioned before, the catalyst particles are formed by thermally induced breakup of a thin metal film during the temperature ramp up and/or annealing processes. Figure 20 illustrates the transformation of a smooth thin metal film into catalytic metal particles. The diameter of the nanotubes depends on the thickness of the evaporated pre-catalytic film on the substrate, because the sizes of the catalyst particles are related to precursor metal layer thickness. For making drawable forests, not only the sizes of the catalyst particles but also the areal densities of these particles are critical factors.

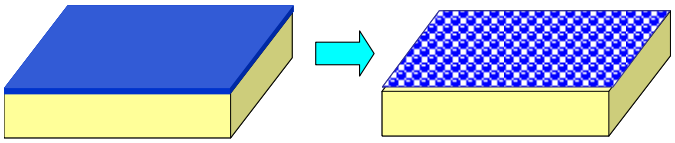

Figure 20. Thin Film Transforms into Small Catalytic Particles during Thermal Processing

We have tried to experimentally determine the relationship between the size and the amount of catalyst particles and thickness of the catalyst thin film by observing changes of surface morphology before and after thermal annealing (Section 3.1). Though we observed morphological changes, it is difficult to measure the number of catalyst particles generated. Also, we cannot in this way determine the fraction of catalyst particles that will be active. For guidance in interpreting results on drawability, we did the following analysis.

In the calculation, we made the following assumptions:

1. The catalyst particles are formed in spherical shape, the total number is n, the radius of each particle is r and its volume is $4/3\pi r^3$.

2. The total volume of the particles is the same as the volume of thin film, namely,

$$st = n\frac{4}{3}\pi r^3 \qquad (1)$$

   Where t is the thickness of the catalyst film and s is the area of the substrate. Here, we ignore the effect of oxidation of the iron film, which may increase the volume of the catalyst film by a factor of 2 or more.

3. All catalyst particles are active. The tubes grow from the catalyst particles, and their outer diameter is $2r$.

Therefore, the coverage of the tubes ξ on the substrate is

$$\xi = \frac{n\pi r^2}{s} \tag{2}$$

Combining above two equations, we have

$$\xi = \frac{3t}{4r}(100\%). \tag{3}$$

The coverage of the tubes on the substrate is a function of the film thickness and the CNT diameter. The results are listed in Table 4 and plotted in Figure 21.

Table 4. Effect of Fe Film Thickness on Coverage of CNTs

	CNT Coverage				
Thickness t (nm)	1	2	3	4	5
Diameter 2r (nm)					
2	75.0%				
3	50.0%				
4	37.5%	75.0%			
5	30.0%	60.0%	90.0%		
6	25.0%	50.0%	75.0%		
7	21.4%	42.9%	64.3%	85.7%	
8	18.8%	37.5%	56.3%	75.0%	93.8%
9	16.7%	33.3%	50.0%	66.7%	83.3%
10	15.0%	30.0%	45.0%	60.0%	75.0%
11	13.6%	27.3%	40.9%	54.5%	68.2%
12	12.5%	25.0%	37.5%	50.0%	62.5%
13	11.5%	23.1%	34.6%	46.2%	57.7%
14	10.7%	21.4%	32.1%	42.9%	53.6%
15	10.0%	20.0%	30.0%	40.0%	50.0%
16	9.4%	18.8%	28.1%	37.5%	46.9%
17	8.8%	17.6%	26.5%	35.3%	44.1%
18	8.3%	16.7%	25.0%	33.3%	41.7%
19	7.9%	15.8%	23.7%	31.6%	39.5%
20	7.5%	15.0%	22.5%	30.0%	37.5%

Because of assumptions (1) and (2), the amount of the catalyst particles calculated is at the lower limit. Even though at this low limit, the calculation results shows more than enough catalyst particles can be generated with a 1-nm thick catalyst film, which is quite surprising.

Previous experimental results show that forests having CNT coverage between 7% and 15% are suitable for spinning nanotubes. From this estimated coverage, a catalyst film 1 nm thick should provide sufficient catalyst particles for obtaining a drawable forest. However, we experimentally find that a catalyst film~3 nm thick is best for obtaining drawable forests comprising ~10-nm-

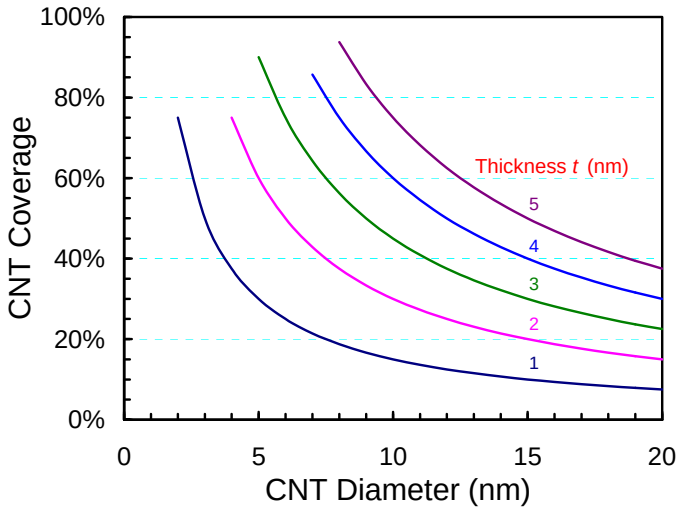

Figure 21. The Relationship among CNT Coverage (% Total Area Occupied by Nanotubes), Thickness of the Catalyst Film, and CNT Diameter

diameter CNTs. This could indicate that more than half of the catalyst particles do not contribute to CNT growth. Considering that most CNTs produced by the chemical vapor deposition process have diameters between 5 and 10 nm, a catalyst film around 2 nm thick might be usefully employed for growing drawable forests. However, irregularities in film thicknesses for such thin metal layer depositions might be problematic.

The main challenge for increasing the drawability of these forests is to effectively increase the amount of active catalyst particles and the activity of the catalyst particles during CVD processing. Keeping catalysts active is the key for increasing the area density of the CNTs. However, it is a challenge to activate more catalyst particles and increase catalyst lifespan, which are important to synthesis of high, drawable forests.

3.3 CNT-Reinforced Transparent Polymer Composite

CNTs belong to a class of nanomaterial that has remarkable physical and mechanical properties. Their superlative mechanical properties make them the filler material of choice for composite reinforcement. CNTs have been dispersed into polymer matrices as filler to reinforce the polymer, but many research results show that the effect of CNT reinforcement is not as large as expected. The main reasons are that it is difficult to disperse a high content of CNTs in a polymer matrix and hard to align CNTs in a composite, and the interaction between CNTs and the polymer is weak. Reinforcement of CNT–polymer composites is mainly influenced by three factors: dispersion of the CNTs in the polymer matrix, interfacial bonding between CNTs and polymer, and alignment of the CNTs in the polymer matrix. When one uses the usual dispersion methods, including the challenges in uniform dispersion and the alignment of CNTs in the polymer matrix, the composite loses transparency at less than 1 wt% content of CNTs because the CNTs in the composite scatter and absorb light. The goal of this work was to make a polymer/CNT composite that not only has enhanced strength, modulus, and toughness, but also is transparent. The method of dispersing CNTs in a polymer matrix to produce a CNT-reinforced composite was unsatisfactory for our project.

In this work, we developed the technology to fabricate CNT–polymer composites. We used poly(methyl methacrylate) (PMMA) as the polymeric matrix. PMMA is a transparent thermoplastic that is often used as a light or shatter-resistant alternative to glass. It is an economical alternative to polycarbonate (PC). PMMA is commonly called acrylic glass, simply acrylic, Perspex or Plexiglas. There are many technical reasons to attempt to make nanocomposites using CNT and PMMA. To apply superior properties of CNT to composites, it is important to disperse CNTs in matrix materials uniformly and to intensify the coherence at the interfaces of CNTs and matrix materials. Several dispersion methods such as melt blending,[13] in-situ polymerization,[14] solution mixing (solvent evaporation),[15,16] and mold injection[17] have been proposed. Those methods show improvement in mechanical properties of the composite. However, the effect of CNT reinforcement was small and the composite was black. Instead of dispersing CNTs into a polymer matrix, we used solid-state processes to produce a prepreg of CNT assembles and embed the CNT prepreg into a polymer matrix through a hot-press process. This process allows us to precisely control the alignment of CNTs and to have high CNT content, as well as to maintain the transparency of the composite. The prepreg of the CNT assembles involves CNT sheets drawn from CNT forest and sheet stacks, CNT strips made from CNT sheets, and CNT yarn arrays fabricated from CNT yarns that are twist spun from CNT forests. The PMMA we chose has features of high strength, high heat resistance, and high clarity. The basic properties are listed in Table 5. The processes developed here are transferable to other transparent polymers, such as PC and polyethylene terephthalate.

Table 5. Properties of the PMMA

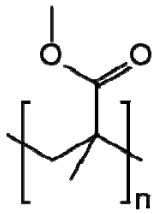

Molecular formula: $(C_5H_8O_2)_n$
Molar mass: varies
Density: 1.17 g/cm^3
Glass transition temperature (T_g): 110 °C
Melting point: 220 °C

Sample Preparation

a. PMMA Sheet

PMMA pellets (Evonik CYRO LLC ACRYLITE 8N Acrylic) from Amco Plastic Materials Inc. were used to make PMMA sheet through a hot-press process. A mold charged with PMMA pellets was placed in a hot press set to reach 220 °C without applying pressure for 30 min (till the plates temperature reached the maximum set temperature). Then 1 metric ton was applied for a few minutes. The hot press was shut off to cool down, and the pressure was maintained till the press reached 80 °C. Then the pressure was released completely from the mold (except the weight of the upper aluminum plate) till it cooled to room temperature. The thickness of the PMMA sheets was controlled between 20–30 μm. The sheet was uniform and transparent, with transmittance around 90% (Fig. 34(a)).

b. PMMA–CNT Composite

PMMA–CNT composites were made by applying CNT assemblies (sheets, strips, or yarns) on top of a PMMA sheet, and then embedding the CNTs into the PMMA matrix by hot-pressing, similar to the process described for making PMMA sheets. The details of each kind of

composite are described in sections 3.3.1, 3.3.2 and 3.3.3. The CNTs used are multi-walled CNTs of ~10 nm diameter and 300–500 μm length.

Property Characterization

a. Optical Property
Ultraviolet–visible (UV-Vis) spectra were recorded with a Cary 5000 UV–Vis–NIR spectrophotometer (Varian, Inc.). Spectra of the samples were scanned with air as background.

b. Structure and Morphology
An optical microscope (Olympus BX40 with CCD camera) was used to evaluate the CNT strips and CNT yarn arrays in PMMA matrices. The CNT sample was observed using SEM and the sample of PMMA–CNT composite was coated with a gold layer before the SEM observation.

c. Mechanical Property
Tensile samples were cut from the hot-pressed PMMA–CNT composite (Figs. 23 and 31). Each sample was weighed by a digital balance and the thickness and width were measured.

Dynamic Mechanical Analysis (DMA) was performed on a DMA Q800 machine (TA Instruments, Inc.), which has 18-N maximum load cell and 0.1-mN accuracy. DMA was used to investigate the tensile properties (strength, modulus, and toughness) of hot-pressed PMMA/CNT composites. The gauge length, film width, and force rate for the tensile test were ~10 mm, 3~4 mm, and 0.5 N/min or 1.0 N/min, respectively. The loading direction is parallel to the direction of CNT alignment. DMA also shows mechanical properties as a function of temperature. For measuring storage modulus and tan δ, DMA was conducted using the film mode with a constant frequency from room temperature to 100 °C at a heating rate of 3 °C/min. The frequency was set at 1, 5, 10, 50, and 100 Hz. After the tensile test, the fracture patterns of the samples were observed using an optical microscope and SEM.

d. Thermal Property
Thermogravimetric Analysis (TGA) was run on a TGA Q50 machine (TA Instruments, Inc.). TGA of various films was conducted in air or in nitrogen at a heating rate of 10 °C/min and the gas flow rate was 60 mL/min. For PMMA/CNT composite, TGA was run in nitrogen from 25 °C to 450 °C and then in air from 450 °C to 800 °C.

For differential scanning calorimetry (DSC), a DSC Q100 apparatus (TA Instruments, Inc.) was utilized. The curves were recorded for the second heating cycle. The glass transition temperature (T_g) and melting point (T_m) of the films were measured by DSC.

3.3.1 CNT Sheets and PMMA–CNT-Sheet Composite

A CNT sheet is a special assembly of CNTs (Section 3.2) drawn from a CNT forest (Fig. 22a). It is very thin, very light, very porous, but robust and strong. Its tensile strength is comparable to that of Kevlar and aluminum sheet. CNT-reinforced polymers attract interest for their potential applications. However, as mentioned in section 3.3, practical applications have been hindered by poor dispersion, lack of alignment of nanotubes, and weak interfacial bonding between CNTs and polymer. Using assembled CNT sheet can eliminate those problems, because the CNTs are well aligned in the sheet and no dispersion is needed. Also, CNTs in the current CNT–polymer material are longer. A CNT sheet is like a preformed fiber network. Because the sheet is made by

solid-state process and is free standing, we are able to place it on the surface of the subject, choose the alignment directions, stack the sheets as desired, and functionalize the CNTs.

The process to make a PMMA/CNT sheet composite is shown in Figure 22b. Free-standing CNT sheets were sandwiched between PMMA sheets and then embedded into the polymer matrix by a hot press. CNT content in the composite is controlled by the number of layers of the CNT sheet. Optical images of the composites are shown in Figure 23. The composite made from two CNT

(a)

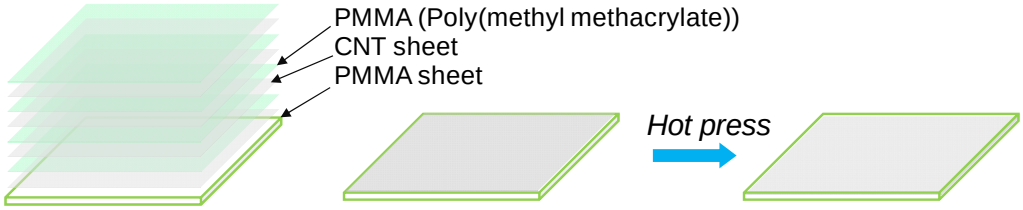

Apply multilayer CNT sheets between PMMA sheets

Hot Press to form PMMA–CNT-sheet composite
(CNT sheets are immersed in PMMA matrix.)

(b)

Figure 22. Schematic Illustration of the Process to Fabricate PMMA/–CNT-Sheet Composite. (a) CNT Sheet Is Drawn from a CNT Forest (b) Illustration of Making PMMA–CNT-Sheet Composite

(a) (b)

Figure 23. Optical Images of PMMA/CNT-Sheet Composites with (a) Two CNT Sheets and (b) Ten CNT Sheets

Colored Marks are beneath the samples of the composite. Samples are 3 cm in diameter sheets per PMMA layer has high transparency when there are. However, the transparency goes down to less than 30% transmittance when the CNT sheets increase to 10 per PMMA layer. Figure 24 shows the CNT sheet transmittance in the UV–visible light range. Transparency of the CNT sheet stack decreases as the number of CNT sheet layers increases.

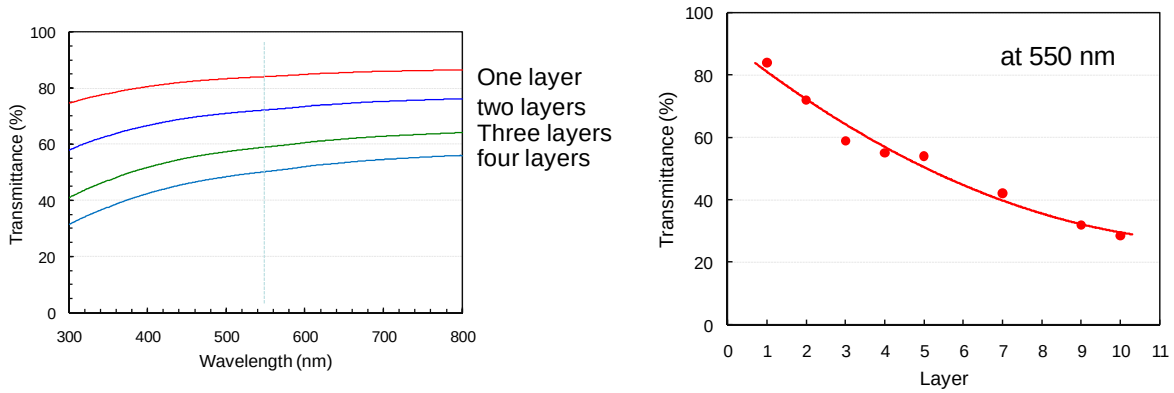

(a) (b)

Figure 24. Optical Properties of CNT Sheets. (a) Transmittance UV–Vis Spectra of CNT Sheets with Different Layers and (b) Transmittance of the Sheets at 550 nm

Two typical SEM images of a PMMA–CNT sheet composite with broken ends are shown in Figure 25. They show clearly that the composite has the structure expected. CNTs are aligned, the alignment is well controlled, and the CNTs are uniformly distributed in the composite (Fig. 23 and Fig. 25). When using six layers of CNT sheet, the content of CNTs in composite is ~0.2 wt% and the modulus of the composite is 1.3 times higher than that of the PMMA sheet. However, the transparency is less than 50 %. Further improving mechanical properties of the composite required that we increase the CNT content and create optical paths at the same time.

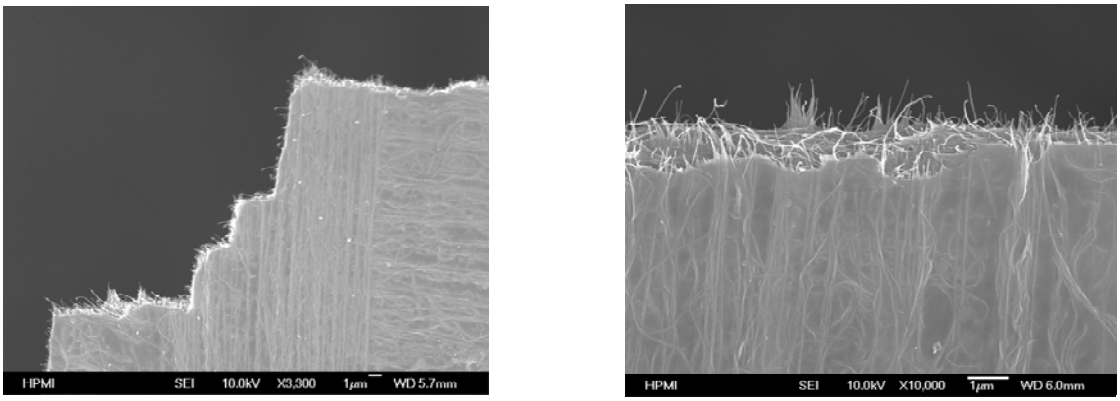

(a) (b)

Figure 25. SEM Images of the PMMA–CNT-Sheet Composites at (a) Low Magnification, (b) Higher Magnification

Directly using CNT sheets as fillers cannot meet our goal: a composite with high strength, high modulus, and high transparency.

3.3.2 CNT Stripes as Filler

For increasing the content of CNTs while keeping transparency of the composite, we tried to locally shrink CNT sheets into strips. Densifying CNT sheets into strips could be a solution because the space between strips is an optical path, and the strips have higher strength than the sheet. Experimentally, we put a sheet on the holder as shown in Figure 26, then formed strips by applying solvent or air flow to the sheet. We were able to control the size of the strips and the spacing between them (Fig. 26). The transmittance is as high as 98%. However, we lost control of the size and spacing of the strips when we added more layers to the sheet. Figure 27 shows images of strips formed from two, four, six, and 10 layers. Although all of these retain very high transmittance, the deviation in size of the strips and the gap between strips increses as the layers increase. Because the strip size and distribution cannot be well controlled, we abandoned this approach. Using the same concept, we fabricated CNT yarns to replace CNT strips.

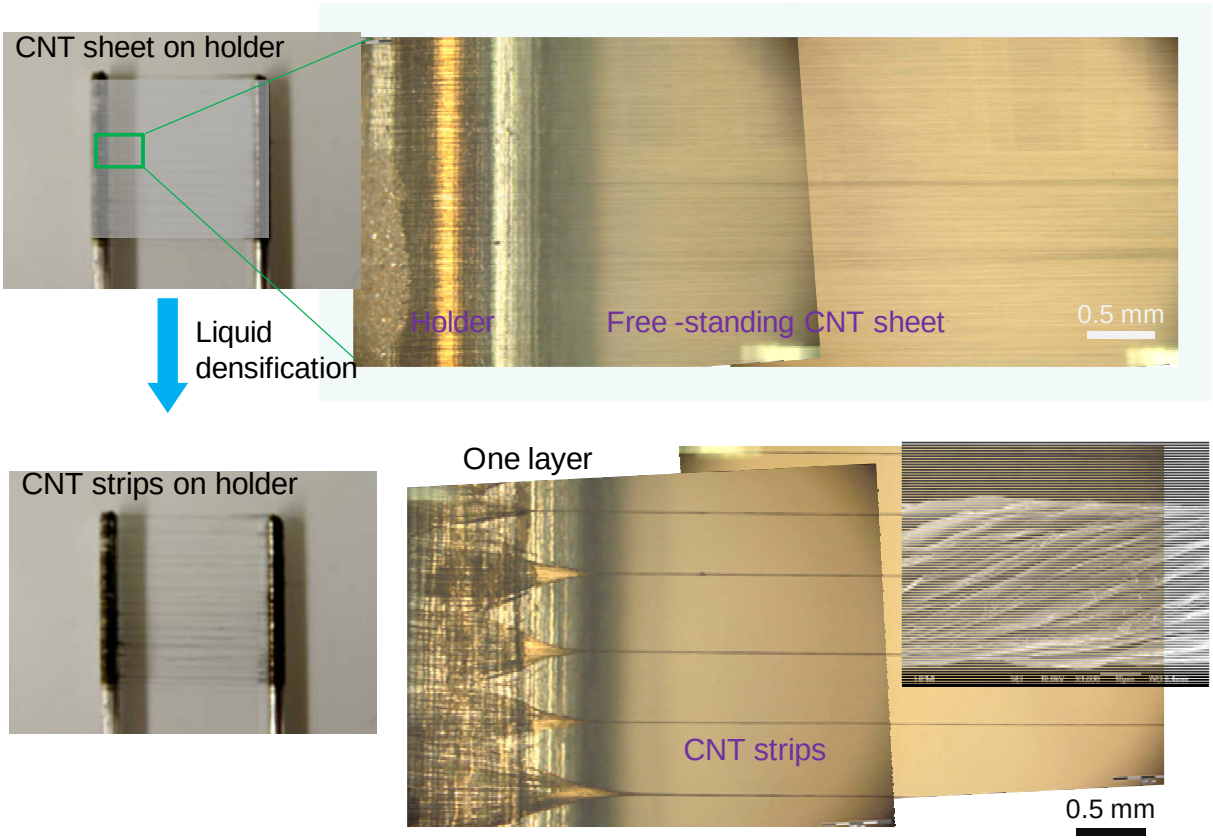

Figure 26. Formation of CNT Strips from CNT Sheet

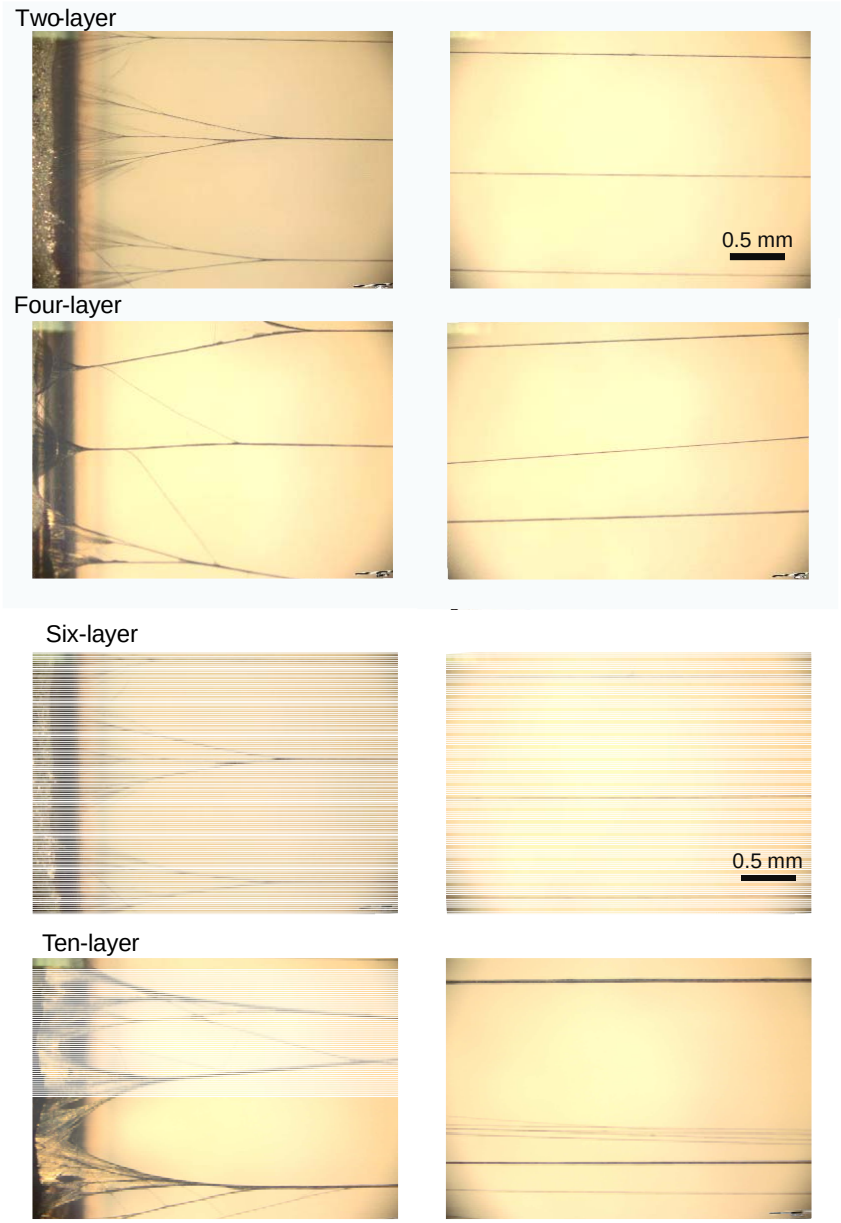

Figure 27. Optical Images of Strips Formed From 2, 4, 6 and 10 Sheet Layers

3.3.3 CNT Yarns and PMMA–CNT-Yarn Composite

CNT yarns are twist spun from a CNT forest. Figure 28a shows a photograph of a yarn that was twist spun from a CNT forest and Figure 28b is a typical SEM image of the yarn. The diameter of the yarn used in the investigation was in the range of 15 μm to 30 μm. Twist spinning assembles the CNTs into a highly organized structure without damaging them or lowering their aspect ratio. Our approach allows us to form well designed CNT networks inside polymer matrices, which meets the fundamental requirements for a filler: high aspect ratio, good distribution in the polymer matrix, good alignment and better interfacial stress transfer.

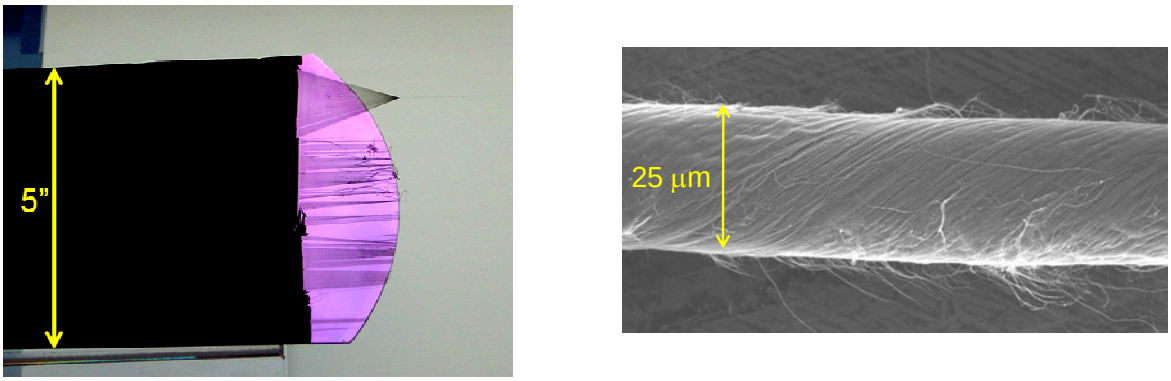

(a) (b)

Figure 28. Twisted-CNT Yarn: (a) Optical Image of a CNT Yarn Twist Spun from a CNT Forest, (b) Typical SEM Image of the CNT Yarn Used in Composites

The engineering stress–strain behavior of PMMA sheet and CNT yarns has been tested and is shown in Figure 29. Absolute values for tensile strength and strain of PMMA sheet are ~40 MPa and 2.7% respectively, similar to the standard values, which indicates that our hot-press process is optimized. The pristine CNT yarn has about 10 times higher strength and 3.5 times longer strain than that of PMMA sheet. It suggests that CNT yarn can be used to reinforce a PMMA matrix. When the yarn was passed through a PMMA–acetone solution, PMMA at least partially infiltrated into the yarn and formed PMMA-coated CNT yarn after drying. Figure 29b shows that the mechanical properties of the yarn are enhanced by the small amount of PMMA infiltration. As a result, PMMA infiltration will help by forming cross-link inside the yarn to limit sliding between CNTs under load. When the CNT yarns are embedded into the PMMA matrix, the PMMA will infiltrate into the CNT yarns, at least on their skin. The filler will have the same strength as the PMMA-coated CNT yarn.

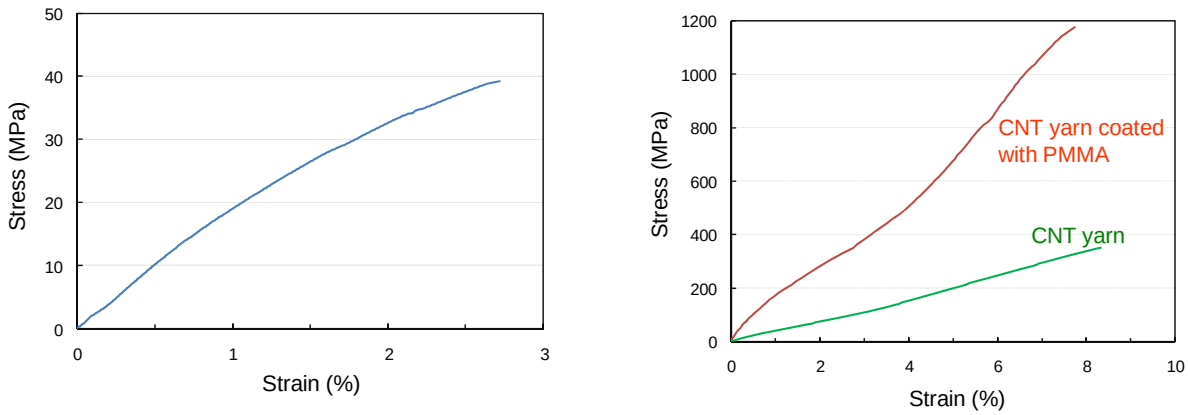

(a) (b)

Figure 29. Tensile Stress–Strain Curves of (a) PMMA Sheet and (b) CNT Yarn and CNT Yarn Coated With PMMA

The optical picture in Figure 30 shows the CNT yarn array and pattern embedded in PMMA matrix. It is important to keep the distribution of the CNT yarns uniform and straight in the PMMA matrix. We developed a process (Figure 31) to maintain the yarn array pattern so that the yarns kept their morphological behavior during hot pressing. Only small amounts of yarn move and stick together during hot pressing. At high CNT content (more CNT yarns, less separation between CNT yarns), it is still a challenge to keep uniform distribution and straightness of the CNT yarns in the polymer matrix.

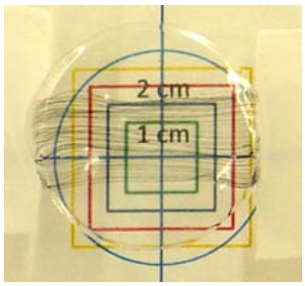

Figure 30. Optical Image Showing That 85 ϕ13 μm CNT Yarns Form an Array and Are Embedded in the PMMA Matrix (CNT Content: 4.7 wt%)

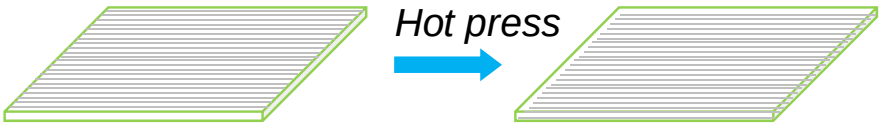

Apply CNT yarn array on PMMA sheets

Form PMMA–CNT-yarn composite (CNT yarns are embedded in the PMMA matrix.)

Figure 31. Schematic Illustration of the Process to Fabricate PMMA–CNT-Yarn Composite

CNT content in composite is controlled by the number of CNT yarns, i.e., the area density of the CNT yarn array. PMMA–CNT-yarn composites were prepared at CNT loadings of 0.8 to 19 wt%. The content weight percent was obtained from TGA. For all these compositions, CNT dispersed uniformly into the PMMA matrix as evidenced by the optical micrographs and SEM images. Figures 32a–c show optical images of samples containing 2.1, 4.4, and 19 wt% CNTs.

TGA was performed to assess the thermal stability of PMMA and PMMA–CNT-yarn composites and the content of CNTs in each composite. As a result, TGA was conducted on PMMA and PMMA–CNT composites in nitrogen from 25 °C to 450 °C and then in air from 450 °C to 800 °C at a heating rate of 10 °C/min. The gas flow rate was 60 mL/min. The TGA curves are shown in Figure 33. From the TG curves it can be seen that the sample weight loss can be divided into two parts. The first weight loss stage is attributed to the loss of PMMA and the second is the loss of CNTs. The CNT content in a composite is obtained as the weight loss between 450 °C and 550 °C. The decomposition temperatures of PMMA and CNTs in

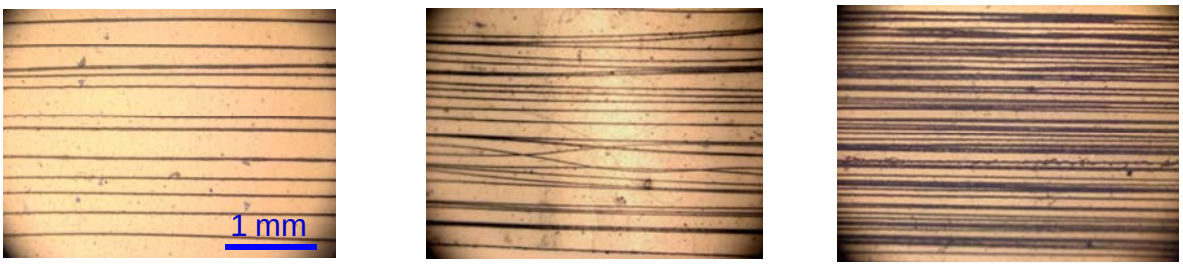

(a) (b) (c)

Figure 32. Optical Images of PMMA–CNT-Yarn Composites Containing (a) 2.1 wt%, (b) 4.4 wt%, and (c) 19 wt% CNT. Images Are in the Same Scale

composites are determined by reading the peak position from the derivative of the weight curves (Fig. 33). The derivative curve for weight data in Figure 33 shows that all these composites have nearly the same PMMA decomposition temperature, 361 °C, as neat PMMA sheet, which indicates that CNTs do not affect PMMA's decomposition in nitrogen. The CNT decomposition temperature shifts to lower temperature as the CNT content decreases.

The UV–vis spectra provide quantitative information concerning the transparency of the film, the presence of CNTs, and the uniformity of CNT distribution. Figure 34a shows that the UV–vis spectra of composite films with CNT contents from 0 to 19 wt% exhibited 40% transmittance and higher in the range of 400 nm to 800 nm. Percent transmittances of composites with different CNT contents at 550 nm are shown in Figure 34b. The transmittance of the composite has an almost linear relationship with the CNT content.

The density of the neat PMMA sheet is 1.18 g/cm^3 and the density of the pristine CNT yarn is around 0.8 g/cm^3. As the CNT content increases, the density of the composite decreases slightly. The density of a composite with 17 wt% CNTs is ~1 g/cm^3.

To examine the influence of nanotubes on deformation and fracture behavior of the polymer films, the DMA was operated under controlled force mode to obtain static stress–strain curves (1 N/min, 25 °C). Figure 35a shows typical engineering stress–strain behavior of PMMA sheet and PMMA–CNT-yarn composite under constant loading rate. The PMMA–CNT-yarn composites show dramatically high tensile strength, which strength increases with increasing content of CNTs. The change of the modulus, strength, and strain of the composite with the CNT content is shown in Figures 35b and 35c.

Compared to the unreinforced PMMA sheets, increasing CNT content increased the modulus of the composite (Fig. 35b). Figure 35c shows that increase of the CNT content also leads to a significant increase in strength of the composite. Both the tensile modulus and the tensile strength increased linearly with increasing nanotube loading; they increased by a factor of 10 and 5, respectively at 17 wt% CNT content, while the strain remained nearly constant (Fig. 35d). This shows that the CNTs in the composite are highly organized and oriented close to the loading direction. Increases in elastic modulus and ultimate strength indicate that nanotubes reinforce the polymer matrix by directly transferring load from nanotube to nanotube and from the polymer to

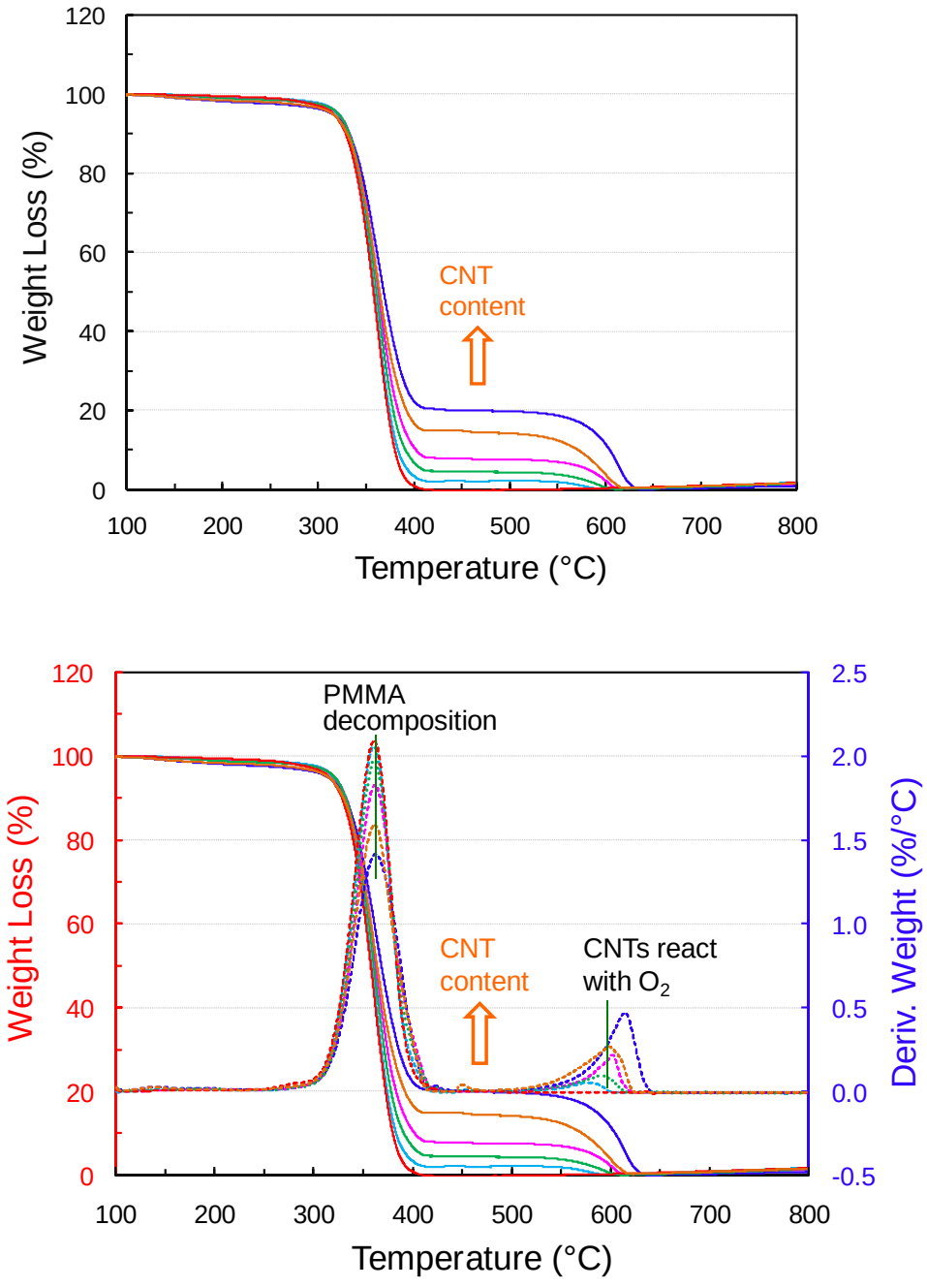

Figure 33. TGA Results of the PMMA–CNT-Yarn Composites

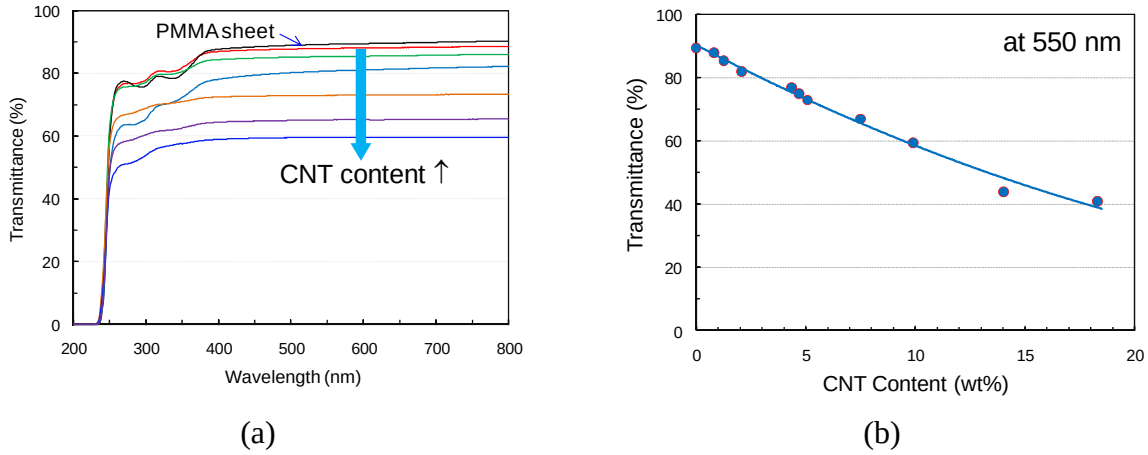

(a) (b)

Figure 34. Optical Properties of Some PMMA–CNT-Yarn Composites. (a) Transmittance UV-Vis Spectra of PMMA and CNT Sheet and (b) Transmittance of the Composites at 550 nm

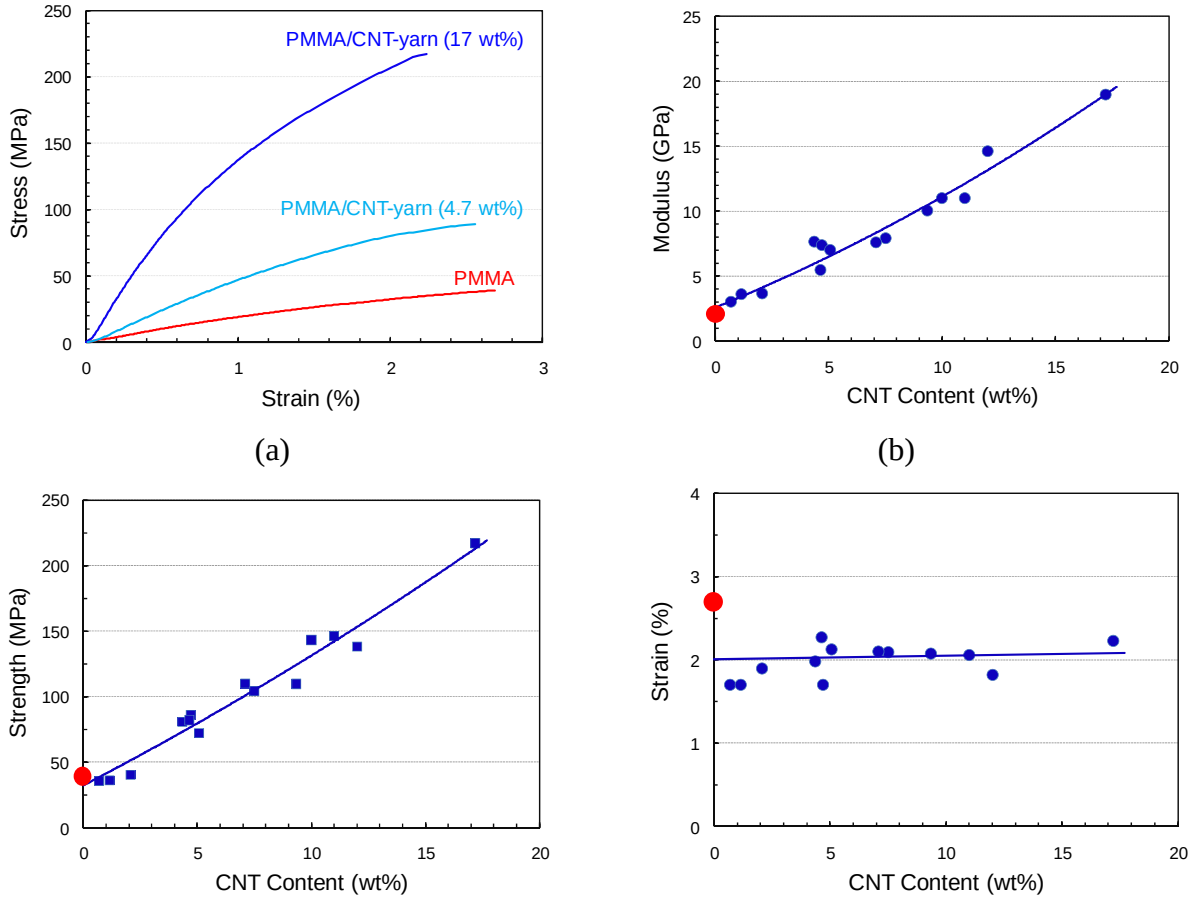

(a) (b)

(c) (d)

Figure 35. Mechanical Properties of PMMA–CNT-Yarn Composites

the nanotubes. In addition, aligned nanotubes resulted in significantly improved ultimate strengths, indicating that there is load transfer between the polymer matrix and the reinforcing nanotubes.

The reinforcement and the rupture behavior of CNT–polymer composite were studied. Figures 36a–c show fracture patterns of the composite after the tensile test. Figure 36c shows the cross-section of the composite. CNT yarns were embedded inside the PMMA matrix. Figure 36b is the SEM image of the fractured end as a ~45° view. The presence of fractured yarns, along with the matrix still adhering to the fractured yarns and nanotubes, indicates good wetting and adhesion of the nanotube yarns to the matrix. The rupture behavior of the composite film under tension, including crazing of the polymer matrix, breakage of CNT yarns (nanotubes), and pullout of CNTs, was observed. They suggest that CNTs reinforce the polymer fibers by hindering extension of crazing, reducing stress concentration, and dissipating energy by pullout (Fig. 36). Distribution of CNT yarns in the polymer matrix and interfacial adhesion between nanotubes and polymers are two major factors that determine the reinforcing effect of CNTs in polymer films.

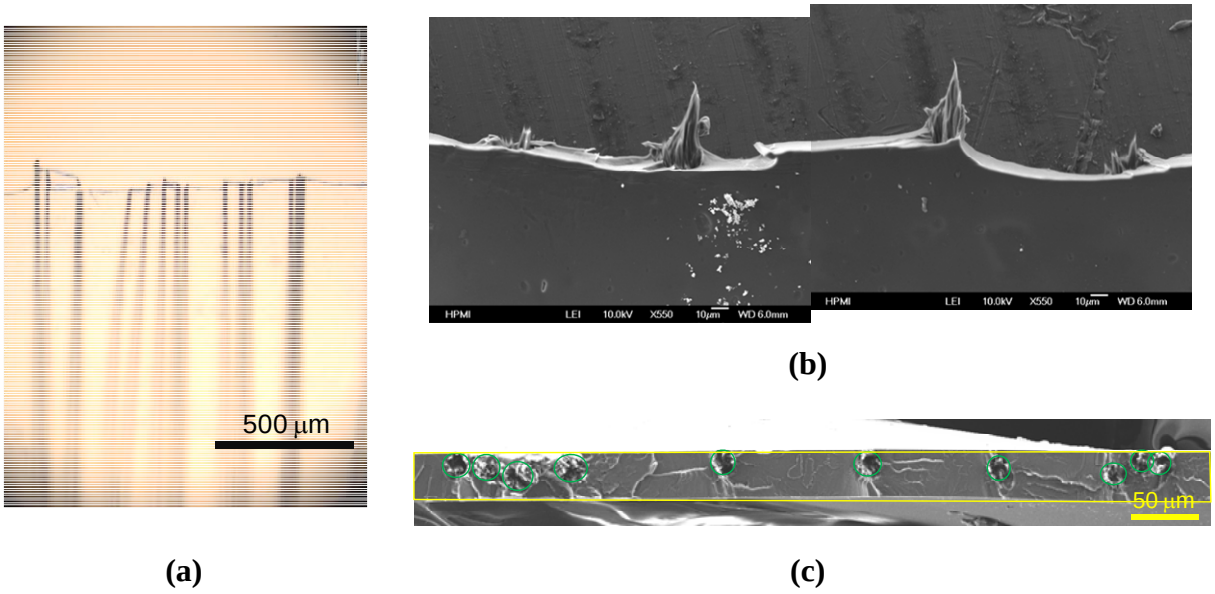

Figure 36. Optical Image (a) and SEM Images (b) and (c) Show the Broken Ends of a PMMA–CNT-Yarn Composite after Tensile Testing

We found that the PMMA–CNT composite with 10 wt% CNT yarns showed an increase of 250% and 500% in tensile strength and modulus, respectively, with a little loss of elongation. When the CNT content increased to 17 wt%, the composite had fivefold increase in strength and 10 fold increase in modulus. Toughness of the composite also improved as CNT content increased. The toughness of the composite with 17 wt% CNT content is up to 11 J/g, 8 times higher than that of a neat PMMA sheet. This approach also keeps over 40% transparency of the composite. It is clear that CNT–yarn arrays effectively enhanced the mechanical properties of the PMMA matrix.

The composite's thermal properties were also investigated by DSC and DMA. DSC endotherms and exotherms of neat PMMA sheet and PMMA–CNT-yarn composite sheet (4.7 wt% CNT content) in a nitrogen atmosphere are shown in Figure 37. T_g of the neat PMMA is 110 °C, which is estimated from the midpoint of a heat capacity peak. T_g changes only slightly with CNT yarn reinforcement. DSC and TGA of a neat PMMA and PMMA–CNT-yarn composites indicate that the thermal stability properties of the matrix are not modified by using CNT yarn as filler. The PMMA–CNT-yarn composite shows a higher value of heat flow, which indicates that the CNT addition lowers the thermal capacity of the composite and increases the intensity of the endotherm and exotherm.

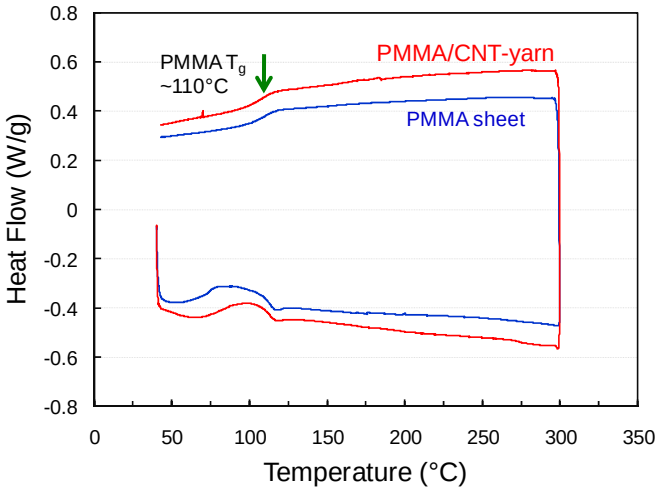

Figure 37. DSC Spectra of a PMMA Sheet and a PMMA–CNT-Yarn Composite.

Figures 38a and 38b show the results of the constant-frequency temperature scan (3 °C/min) on the elastic and damping behavior of the films. The frequency was set at 1, 5, 10, 20, 50, and 100 Hz. The films show higher modulus at higher frequency. The addition of nanotubes results in a moderate increase in the elastic storage modulus over the unreinforced PMMA. As compared to the neat PMMA sheet, the storage modulus at 25 °C of the composites increased 2.4 times when the CNT content was 4.4 wt%. The difference in loss modulus between the neat and CNT reinforced PMMA sheets was small, especially at lower frequency.

The resistance to creep of a PMMA–CNT-yarn composite with 4.4 wt% CNT content was tested by DMA. The tensile load was set at stresses of 5, 15, 25 and 50 MPa. 50 MPa is about 2/3 of the ultimate stress of this composite. Under each loading, the temperature was ramped from room temperature to 100 °C at the rate of 3 °C/min. Under each loading and during the temperature scan, the change in gauge length of the sample was monitored. The results are shown in Figure 39. The length change is less than 0.05% for each test and the length change is not elongation. Further tests are needed for us to understand the composite's creep behavior.

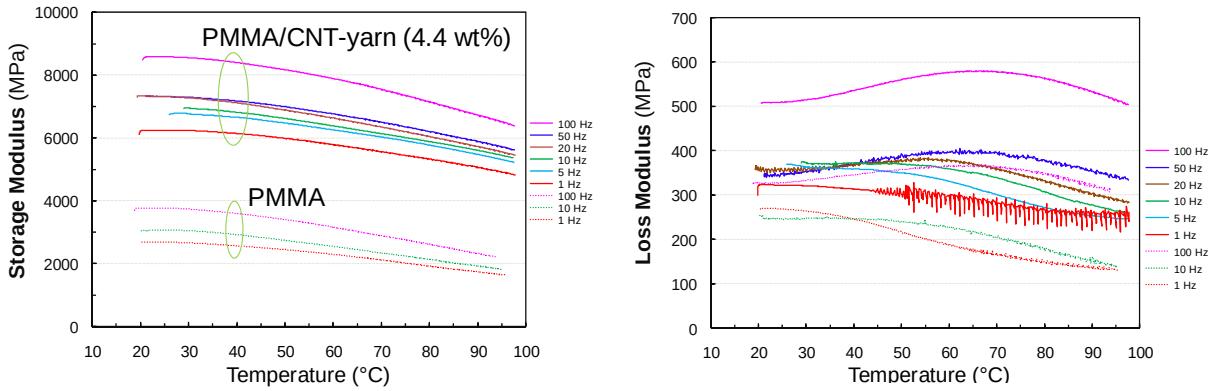

(a) (b)

Figure 38. Storage Modulus (a) and Loss Modulus (b) of PMMA and a PMMA/CNT-Yarn Composite as a Function of Temperature at Different Frequencies

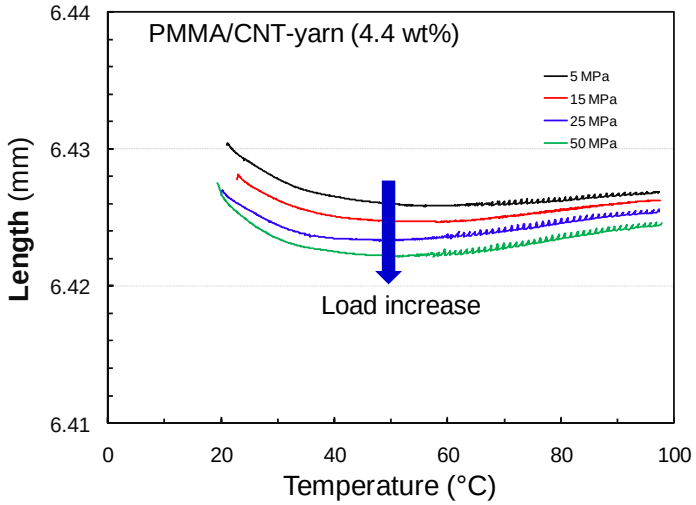

Figure 39. Length of the PMMA–CNT-Yarn Composite with 4.4 wt% CNT Content under Different Loadings and Temperatures

The results demonstrated that using the highly organized CNT assemblies to form CNT yarns for use as filler is an effective and efficient way to improve the properties of polymeric composite while keeping the transparency of the composite . One question is raised—were the ideal properties of the composite achieved? To answer this question, we calculated the ideal strength and modulus based on the structure of the composite and the properties of PMMA and CNT yarn.

Figure 40 shows a geometric illustration of uniaxial stressing of a composite with continuous yarn reinforcement and all the terms used in calculation. As shown in Figure 40, the stress parallel to the direction of yarn alignment in the PMMA–CNT-yarn composite is a typical uniaxial stressing of such a material.

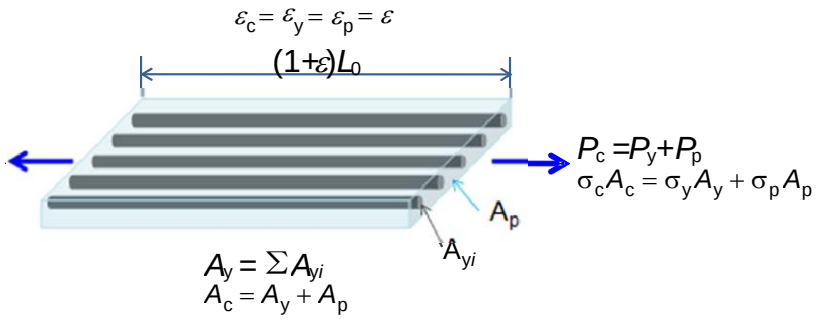

A	area
M	mass
V	volume
ρ	density
P	load
σ	tensile stress
ε	tensile strain
E	modulus
X	CNT content (mass fraction) in the composite

The subscripts c, y, and p, are used to represent composite, CNT yarn and polymer matrix, respectively.

Figure 40. Illustration of Uniaxial Stressing of a Composite with Continuous Yarn Reinforcement

The PMMA–CNT-yarn composite is formed from two components, CNT yarn and PMMA matrix. The mass and volume of the composite are the sums of those of the components, yarn and PMMA matrix. The cross-sectional area of the composite is the sum of those of the two components. Since the strain at fracture of the composite is smaller than that of both PMMA sheet (Fig. 35d) and CNT yarns (Fig. 29) and from the fracture pattern observed, it is clear that the matrix (PMMA) is intimately bonded to the reinforced CNT yarns. Therefore, the strain of both the matrix and the yarns are the same. That is,

$$\varepsilon_c = \varepsilon_y = \varepsilon_p \tag{4}$$

It is also apparent that the load carried by the composite, P_c, is the simple sum of loads carried by each component:

$$P_c = P_y + P_p \tag{5}$$

From the definition of the engineering stress, each load is equal to a stress times an area; that is

$$\sigma_c A_c = \sigma_y A_y + \sigma_p A_p \tag{6}$$

Therefore, the stress of the composite σ_c is

$$\sigma_c = \sigma_y \frac{A_y}{A_c} + \sigma_p \frac{A_p}{A_c} \tag{7}$$

Since the cross-section area of the composite $A_c = A_y + A_p$, we have

$$\sigma_c = \sigma_y \frac{A_y}{A_c} + \sigma_p \left(1 - \frac{A_y}{A_c}\right) = \left(\sigma_y - \sigma_p\right)\frac{A_y}{A_c} + \sigma_p \quad (8)$$

Because of the geometry of the composite of Figure 40, the area fraction of the CNT yarns in the cross-section area is also the volume fraction in the composite. Therefore, from Equation 5 we have

$$\sigma_c = \left(\sigma_y - \sigma_p\right)\frac{V_y}{V_c} + \sigma_p \quad (9)$$

The density of the composite, CNT yarn in the composite, and polymer matrix is $\rho_c = \frac{M_c}{V_c}$, $\rho_y = \frac{M_y}{V_y}$, and $\rho_p = \frac{M_p}{V_p}$, respectively. Using mass, volume, and density relationship, the stress of the composite is related with the content of CNTs in the composite:

$$\sigma_c = \left(\sigma_y - \sigma_p\right)\frac{M_y}{M_c}\frac{\rho_c}{\rho_y} + \sigma_p = \left(\sigma_y - \sigma_p\right)\frac{\rho_c}{\rho_y}X + \sigma_p \quad (10)$$

The density of the composite, ρ_c, is determined by the densities of the CNT yarn and polymer matrix in the composite and the CNT mass fraction X (CNT content):

$$\rho_c = \frac{M_c}{V_c} = \frac{M_c}{V_y + V_p} = \frac{M_c \rho_y \rho_p}{M_y \rho_p + M_p \rho_y} = \frac{\rho_y \rho_p}{X\rho_p + (1-X)\rho_y} = \frac{\rho_y \rho_p}{(\rho_p - \rho_y)X + \rho_y} \quad (11)$$

Using Equation 8 to replace the ρ_c in Equation 7, the stress of the composite can be described by the densities and stress of CNT yarn and polymer as well as the content of CNTs in the composite:

$$\sigma_c = \left(\sigma_y - \sigma_p\right)\frac{\rho_p}{(\rho_p - \rho_y)X + \rho_y}X + \sigma_p \quad (12)$$

The modulus of the composite is determined by the modules of CNT yarn and polymer as well as the content of CNTs. At elastic deformation range, we have $\varepsilon_c = \frac{\sigma_c}{E_c} = \varepsilon_y = \frac{\sigma_y}{E_y} = \varepsilon_p = \frac{\sigma_p}{E_p}$.
Combining Equations 1 and 3 gives

$$E_c \varepsilon_c A_c = E_y \varepsilon_y A_y + E_p \varepsilon_p A_p \quad (13)$$

Namely,

$$E_c A_c = E_y A_y + E_p A_p \quad (14)$$

The modulus of composite will be

$$E_c = E_y \frac{A_y}{A_c} + E_p \frac{A_p}{A_c} \quad (15)$$

By using the relationships among mass, volume, density, and mass fraction, the modulus of the composite becomes

$$E_c = E_y - (E_y - E_p)\frac{\rho_y(1-X)}{(\rho_p-\rho_y)X+\rho_y} \quad (16)$$

According to Equation 9, the calculated strength of the composite as a function of CNT content is shown in Figure 41. The parameters used in calculation: PMMA strength and density are 40 MPa and 1.17 g/cm^3, respectively; the strength of CNT yarn is 1100 MPa. Since CNT yarns are embedded inside the PMMA matrix, we treat the yarn as PMMA-coated yarn; the strength of 1100 MPa is from Figure 29b. The pristine CNT yarn has a density around 0.8 g/cm^3. When the yarn is embedded in the PMMA matrix under pressure, it is believed that its density will increase because of the polymer infiltration and shrinkage in diameter. However, the density should exceed1.1 g/cm^3 (the density of the composite is less than 1.12 g/cm^3). Therefore, density of the yarn varies from 0.8 to 1.1 g/cm^3 in the calculation. Red dots and line in Figure 41 are experimental results from Figure 35c.

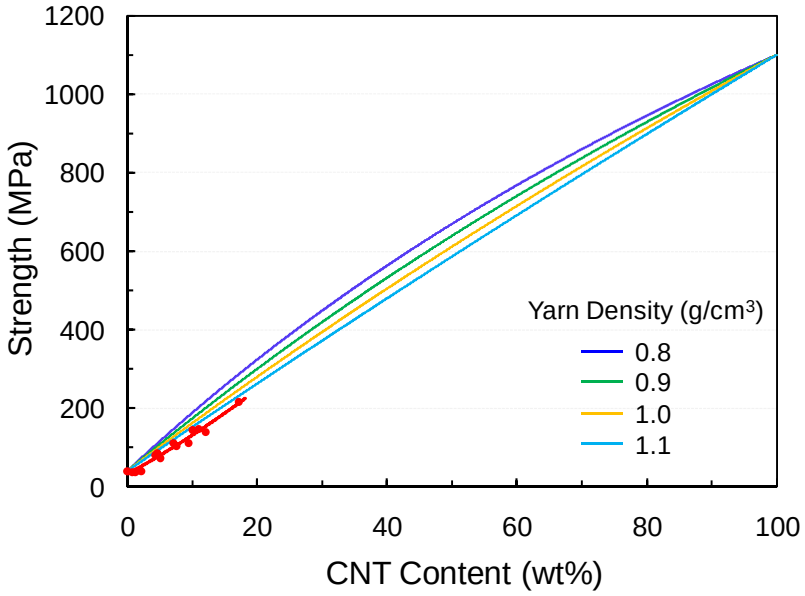

Figure 41. Strength of the Composite vs. CNT Content

The calculated modulus of the composite based on Equation 13 is plotted in Figure 42 as a function of CNT content. The modulus and density of PMMA sheet used in calculation are 2.07 GPa and 1.17 g/cm^3, respectively; the modulus of the PMMA-coated CNT yarn is 90 GPa, obtained from the stress–strain curve in Figure 29b. Density of the yarn varies from 0.8 to 1.1 g/cm^3 in the calculation. The red dots and line in Figure 42 are experimental results from Figure 35b.

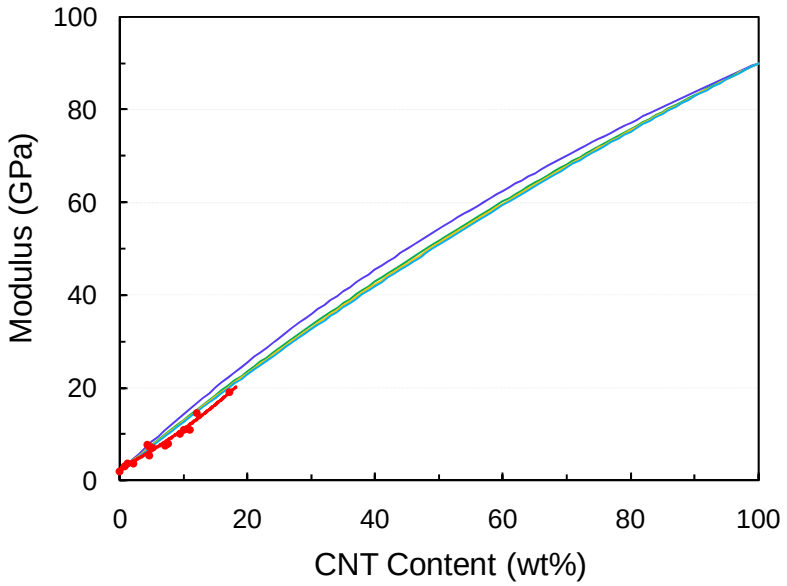

Figure 42. Modulus of the Composite vs. CNT Content

The calculation proved that our process of composite fabrication is well developed and the geometry is an ideal application to a composite. The high modulus and strength of the CNT yarns are effectively transmitted to the composite as a whole. The fabrication of transparent polymer–nanotube composites may prove to be a useful tool in developing transparent composites with enhanced optical, electrical and mechanical properties. The primary objective of this work was to develop and demonstrate a new, effective method to prepare CNT-reinforced transparent polymer composites. These goals have all been met.

If we take the density and modulus of the yarn as 1.1 g/cm^3 and 90 GPa, respectively, the volume fraction of the CNTs will be ~ 20 vol% when the mass fraction of CNTs is 17 wt%. Then the fractional loading on CNT yarn will be about 92%. That is, nearly the entire uniaxial load is carried by CNT yarn. It is obvious that increasing the strength and modulus of the filler, CNT yarn, will reinforce the polymer matrix more efficiently and effectively, and deliver a high–strength, high–modulus, transparent composite. To improve CNT yarns' properties is important. Further work is needed to evaluate the method for fabricating thinner CNT yarns, assemble them into ropes, and apply them to other polymers that have higher strength and strain, such as PC. The results achieved in this work are encouraging and suggest that using a well-organized CNT assembly and following well-defined methodologies offers promise for achieving highly reinforced, transparent, polymer composites suitable for blast-resistant applications.

4. CONCLUSIONS

The following points summarize the key accomplishments and significant conclusions that can be drawn from the current program:

1. The parameters— catalyst formation, catalyst film thickness, catalyst particle size, buffer layers, process temperature, ramp time, gases partial pressure, and growth time—that affectthe growth of CNT forests were investigated.. Forests aver a millimeter high were successfully produced by using C_2H_4 as the carbon source gas.
2. Drawable CNT forests have been achieved in large areas by using both acetylene and ethylene processes. It is possible to further optimize the process and improve the drawability.
3. The relationships among forest area density, CNT coverage, and drawability were explored. It was found that a strong selectivity exists between the catalyst and carbon source. Optimizing catalyst structure is extremely important.
4. The processes are developed to produce *CNT sheets* in which CNTs are well aligned, *CNT strips* in which CNTs are locally densified to form bundles for better load transfer between CNTs, and *CNT yarns*, which are twist spun from forests and have highly organized structure. All of these CNT structures can be used as fillers in polymeric matrices.
5. The processing–nanostructure–property relationships of the resultant CNT–polymer materials are explored and revealed. The high-strength, high-heat-resistance, and high-clarity PMMA was used as a transparent polymer matrix for us to obtain the relationship of optical and mechanical properties with the CNT content.
6. The processes for making PMMA–CNT composites are developed. These processes can be applied to other polymeric matrix.
7. The properties of PMMA–CNT composites are characterized. It is found that CNT yarn arrays are an effective way to control the CNT structure and content in composites, the best way to reinforce the polymer composite andwhile keep high-level transparency of the composite.
8. Reinforced PMMA–CNT-yarn composites were prepared. The modulus and strength of the composite linearly increase with the increase of CNT content. When CNT content is 17 wt%, the modulus of composite is 10 times, strength is 5 times, and the toughness is 8 times higher than that without CNTs (neat PMMA sheet). Further, the composite has more than 40% transmittance even when the CNT content is 19 wt%. To increase the content of CNT yarns can further improve mechanical properties of the polymer/CNT composite without disturbing its thermal properties.
9. Calculation was performed to evaluate the experimental results and predict the composite's properties. This demonstrated that using a highly organized CNT assembly, such as CNT yarns, as filler is an efficient way to improve the properties of polymeric composite while keeping the transparency of the composite.

5. RECOMMENDATIONS

Although many productive conclusions have been obtained in the present study, some aspects of this study need further investigation. Some suggestions for future studies are listed below.

1. CNT synthesis process is important to obtain long, high- quality CNTs. Process improvement and optimization research needs to be continued.

2. There is plenty of room to further increase the mechanical properties of polymer–CNT-yarn composites. It involves the following research:
   - Optimizing the CVD process to synthesis longer CNTs, which will dramatically increase mechanical and transport properties by proportionally decreasing nanotube chain-end concentration. Longer CNTs with fewer defects are essential for improving electrical and mechanical strength of CNTs and CNT–polymer composites.
   - optimizing the fabrication process and morphologies of CNT yarns to increase their mechanical properties,
   - improving the uniformity of distribution of the CNT yarn array in polymer matrices,
   - optimizing the hot-press process to lower the number of defects inside the polymer matrix, especially the voids and micro-cracks, and
   - increasing the interactions between polymer and CNTs.

3. The polymer used in this project, PMMA, is relatively brittle material. Its strain is less than that of CNT yarns. Using a polymer with higher strain, such as PC, will be a better approach to develop composites with not only high strength but also high toughness. Further research on producing PC–CNT-yarn composite is necessary.

6. REFERENCES

1. P.A. Buchan, J.F. Chen, "Blast Resistance of FRP Composites and Polymer Strengthened Concrete and Masonry Structures - A State-of-the-Art Review," *Composites, Part B*, 38, 509 (2007).
2. M.S. Dresselhaus, G. Dresselhaus, P.Avouris, "Carbon Nanotubes: Synthesis, Structure, Properties and Applications," *Springer Verlag*, the First Edition, 2001.
3. M.S. Arnold, A.A. Green, J.F. Hulvat, S.I. Stupp and M.C. Hersam, "Sorting Carbon Nanotubes by Electronic Structure Using Density Differentiation," *Nature Nanotechnology*, 1, 60-65 (2006).
4. D. Tasis, N. Tagmatarchis, A. Bianco and M. Prato, "Chemistry of Carbon Nanotubes," *Chem Rev* 106, 1105 (2006).
5. T. W. Chou, E.T. Thostenson, Z.F. Ren. "Advances in the Science and Technology of Carbon Nanotubes and Their Composites: A Review," *Composites Science and Technology*, 61, 1899 (2001).
6. E.T. Thostenson and T.W. Chou. "Carbon Nanotube Networks: Sensing of Distributed Strain and Damage for Life Prediction and Self-Healing," *Advanced Materials*, 18, 2837-2841 (2006).
7. M. Pulickel, M. Ajayan and James M. Tour, "Nanotube Composites," *Nature*, 447, 1066 (2007).
8. H.D. Wagner, "Nanotube-Polymer Adhesion: A Mechanics Approach," *Chem Phys Lett*, 361, 57 (2002).
9. M. Zhang, S. Fang, A.A. Zakhidov, S.B. Lee, A.E. Aliev, C.D. Williams, K.R. Atkinson, and R.H. Baughman, "Strong, Transparent, Multifunctional Carbon Nanotube Sheets," *Science* 309, 1215 (2005).
10. H.J. Leong, et al. "High-Yield Catalytic Synthesis of Thin Multiwalled Carbon Nanotubes," *J. Phys. Chem*. B 108, 17695-17698 (2004).
11. S.C. Lyu, et al. "Large-Scale Synthesis of High-Quality Single-Walled Carbon Nanotubes by Catalytic Decomposition of Ethylene," *J. Phys. Chem*. B 108, 1613-1616 (2004).
12. S. Fan, M.G. Chapline, N.R. Franklin, T.W. Tombler, A.M. Cassell and H. Dai. "Self-Oriented Regular Arrays of Carbon Nanotubes and Their Field Emission Properties," *Science*, 283, 512-514 (1999).
13. H.M. Christen, A.A. Puretzky, H. Cui, K. Belay, P.H. Fleming, D.B. Geohegan and D.H. Lowndes, "Rapid Growth of Long, Vertically Aligned Carbon Nanotubes Through Efficient Catalyst Optimization Using Metal Film Gradients," *Nano Lett.* 4, 1939-1942 (2004).
14. W.Z. Li, S.S. Xie, L.X. Qian, B.H. Chang, B.S. Zou, W.Y. Zhou, R.A. Zhao and G.Wang. "Large-Scale Synthesis of Aligned Carbon Nanotubes," *Science*, 274, 1701-1703 (1996).
15. A.J. Hart and A.H. Slocum, "Rapid Growth and Flow-Mediated Nucleation of Millimeter-Scale Aligned Carbon Nanotube Structures From a Thin-Film Catalyst," *J. Phys. Chem. B* 110, 8250-8257 (2006).
16. K. Hata, D.N. Futaba, K. Mizuno, T. Namai, M. Yumura and S. Iijima, "Water-Assisted Highly Efficient Synthesis of Impurity-Free Single-Walled Carbon Nanotubes," *Science* 306, 1362-1364 (2004).
17. Z. Jin, K.P. Pramoda, G. Xu, and S.H. Goh, "Dynamic Mechanical Behavior of Melt-Processed Multi-Walled Carbon Nanotube/Poly(methyl methacrylate) Composites," Chemical Physics Letters, 337, 43-47 (2001).

18. Z. Jia, Z. Wang, C. Xu, J. Liang, B. Wei, D. Wu, S. Zhu, “Study on Poly(methyl methacrylate)/Carbon Nanotube Composites,” Materials Science and Engineering : A271, 395-400 (1999).
19. C. Stéphan, T.P. Nguyen, M. Lamy de la Chapelle, S. Lefrant, C. Journet, and P. Bernier, “Characterization of Single-Walled Carbon Nanotubes-PMMA Composites,” Synthetic Metals, 108, 139-149 (2000).
20. K. H. Kim and W. H. Jo, “Improvement of Tensile Properties of Poly(Methyl Methacrylate) by Dispersing Multi-Walled Carbon Nanotubes Functionalized with Poly(3-Hexylthiophene)-Graft-Poly(Methyl Methacrylate),” Composites Science and Technology 68, 2120-2124 (2008).
21. W.-J. Lee, S.-E. Lee, and C.-G. Kim, “The Mechanical Properties of MWNT/PMMA Nanocomposites Fabricated by Modified Injection Molding,” Composite Structures, 76, 406–410 (2006).
22. L.-Q. Liu and H. D. Wagner, “A Comparison of the Mechanical Strength and Stiffness of MWNT-PMMA and MWNT-epoxy Nanocomposites,” Composite Interfaces, 14, 285–297 (2007).

APPENDIX

List of Publications and Presentations
Based in Whole or in Part on Results from the Current Program

Publications:

1. Mei Zhang and Jian Li, “Carbon Nanotube in Different Shapes,” *Materials Today* 12, 12-18 (2009). (Invited review paper; the most downloaded paper of the journal according to ScienceDirect Top-25 Hottest Articles July - September 2009 and October-December 2009).
2. Mei Zhang, Hang Zhang, Richard Liang, Chuck Zhang, Ben Wang, and Dave Scanland, "Transparent Polymeric Composite Reinforced by Carbon Nanotubes," submitted to *Journal of Advanced Materials.*

Presentations:

1. Mei Zhang, “Synthesis of Carbon Nanotubes in Different Shapes: Straight, Wavy, and Spiral,” *MRS Fall Meeting* (Boston, MA, Dec. 1-5, 2008).
2. Mei Zhang, Jian Li, Chuck Zhang, and Ben Wang, “Nanomanufacturing of Carbon Nanotube Array--- The Effect of Catalyst,” *IIE Annual Conference and Expo 2009* (Miami, FL, May 30-June 3, 2009).
3. Mei Zhang, Farag Abdelslam, Chuck Zhang, and Ben Wang, “Carbon Nanotube Assembly for Flexible Transparent Electrodes,” *MRS Fall Meeting* (Boston, MA, Nov. 30-Dec. 4, 2009).
4. Mei Zhang, Hang Zhang, Richard Liang, Chuck Zhang, Ben Wang, and Dave Scanland, "Transparent Polymeric Composite Enhanced by Carbon Nanotubes," *2010 NanoTechnology for Defense Conference* (Atlanta, GA, May 3-6, 2010).
5. Mei Zhang, Hang Zhang, Richard Liang, Chuck Zhang, and Ben Wang, "Polymeric Composite Enhanced by Carbon Nanotube Yarns," *2010 AIChE Annual Meeting* (Salt Lake City, UT, Nov. 7-12, 2010). (accepted)
6. Mei Zhang, Hang Zhang, Richard Liang, Chuck Zhang, Ben Wang, “Transparent Polymeric Composite Reinforced by Carbon Nanotube Yarns,” *MRS Fall Meeting* (Boston, MA, Nov. 29-Dec. 3, 2010). (submitted)

LIST OF ACRONYMS, ABBREVIATIONS AND SYMBOLS

Acronym/ Abbreviation	Description
AFM	atomic force microscopy
AFRL	Air Force Research Laboratory
CNT	carbon nanotube
CVD	chemical vapor deposition
DMA	dynamic mechanical analysis
DSC	differential scanning calorimetry
FRP	fiber-reinforced polymer
GPa	gigapascal
in.	inch(es)
J/g	joules per gram (unit of energy content)
min	minute(s)
mN	millinewton(s)
MPa	megapascal(s)
N	newton(s)
nm	nanometer(s)
PC	polycarbonate
PET	polyethylene terephthalate
PMMA	poly (methyl methacrylate)
rms	root-mean-square
sccm	standard cubic centimeters per minute
SEM	scanning electron microscopy
TEM	transmission electron microscopy
TGA	thermogravimetric Analysis
UV-Vis-NIR	ultraviolet– visible–near infrared
μm	micrometer(s)

Symbol	Description
A	cross-section area
Al	Aluminum
Al_2O_3	Alumina
Ar	argon
C_2H_2	Acetylene
C_2H_4	Ethylene
E	Young's modulus, MPa or GPa
Fe	Iron
He	Helium
M	mass, g
N	number of catalyst particels
O_2	Oxygen
P	load, N
Si	Silicon
SiO_2	Silicon Dioxide
T	temperature
T_g	glass transition temperature
s	area of the substrate
t	thickness of the catalyst film
V	volume
X	CNT content (mass fraction) in the composite
σ	stress, MPa
ε	Strain, %
ρ	Density, g/cm^3
ξ	Coverage of the tubes on the substrate

The subscripts to the symbols, c, y, and p, are used to represent composite, CNT yarn, and polymer matrix, respectively.

1. P.A. Buchan, J. F. Chen, "Blast resistance of FRP composites and polymer strengthened concrete and masonry structures - A state-of-the-art review", *Composites, part B*, **38**, 509 (2007).
2. M.S. Dresselhaus, G. Dresselhaus, P.Avouris, "Carbon nanotubes: synthesis, structure, properties and applications," *Springer Verlag*, the First Edition, 2001.
3. M.S. Arnold, A.A. Green, J.F. Hulvat, S.I. Stupp and M.C. Hersam, "Sorting carbon nanotubes by electronic structure using density differentiation," *Nature Nanotechnology*, 1, 60-65 (2006).
4. D. Tasis, N. Tagmatarchis, A. Bianco and M. Prato, "Chemistry of carbon nanotubes", *Chem Rev* 106, 1105 (2006).
5. T. W. Chou, E. T. Thostenson, Z. F. Ren. "Advances in the science and technology of carbon nanotubes and their composites: A review," *Composites Science and Technology*, 61, 1899 (2001).
6. E. T. Thostenson. "Carbon nanotube network: Sensing of distributed strain and damage for life prediction and self-healing," *Advanced Materials*, 18, (2006).
7. M. Pulickel, M. Ajayan and James M. Tour, "Nanotube composites," *Nature*, 447, 1066 (2007).
8. H.D. Wagner, "Nanotube-polymer adhesion: a mechanics approach", *Chem Phys Lett*, 361, 57 (2002).
9. M. Zhang, S. Fang, A. A. Zakhidov, S. B. Lee, A. E. Aliev, C. D. Williams, K. R. Atkinson, and R. H. Baughman, "Strong, Transparent, Multifunctional Carbon Nanotube Sheets", *Science* 309, 1215 (2005).
10. S. C. Lyu, et al. . *J. Phys. Chem*. B 108, 1613 (2004).
11. S. Fan, M. G. Chapline, N. R. Franklin, T. W. Tombler, A. M. Cassell and H. Dai, *Science* **283**, 512-514 (1999).
12. K. Hata, D. N. Futaba, K. Mizuno, T. Namai, M. Yumura and S. Iijima, *Science* 306, 1362-1364 (2004).
13. Z. Jin, K. P. Pramoda, G. Xu, and S. H. Goh, "Dynamic Mechanical Behavior of Melt-Processed Multi-Walled Carbon Nanotube/Poly(Methyl Methacrylate) Composites," Chemical Physics Letters, 337, 43-47 (2001).
14. Z. Jia, Z. Wang, C. Xu, J. Liang, B. Wei, D. Wu, S. Zhu, "Study on Poly(Methyl Methacrylate)/Carbon Nanotube Composites," Materials Science and Engineering : A271, 395-400 (1999).
15. C. Stéphan, T. P. Nguyen, M. Lamy de la Chapelle, S. Lefrant, C. Journet, and P. Bernier, "Characterization of Singlewalled Carbon Nanotubes-PMMA Composites," Synthetic Metals, 108, 139-149 (2000).
16. K. H. Kim and W. H. Jo, "Improvement of Tensile Properties of Poly(Methyl Methacrylate) by Dispersing Multi-walled Carbon Nanotubes Functionalized with Poly(3-Hexylthiophene)-Graft-Poly(Methyl Methacrylate)," Composites Science and Technology 68, 2120-2124 (2008).
17. W.-J. Lee, S.-E. Lee, and C.-G. Kim, "The mechanical properties of MWNT/PMMA nanocomposites fabricated by modified injection molding," Composite Structures, 76, 406–410 (2006).

18. L.-Q. Liu and H. D. Wagner, “A comparison of the mechanical strength and stiffness of MWNT-PMMA and MWNT-epoxy nanocomposites,” Composite Interfaces, 14, 285–297 (2007).